The University of Sydney

School of Civil Engineering
Sydney NSW 2006
AUSTRALIA

http://www.civil.usyd.edu.au/

Environmental Fluids/Wind Group

Random Wave-Induced Seabed Response

Research Report No R864

Haijiang Liu, BE ME PhD
Dong-Sheng Jeng, BE ME PhD

April 2006

ISSN 1833-2781

The University of Sydney

School of Civil Engineering
Environmental Fluids/Wind Group
http://www.civil.usyd.edu.au/

Random Wave-Induced Seabed Response

Research Report No R864

Haijiang Liu, BE ME PhD
Dong-Sheng Jeng, BE ME PhD

April 2006

Abstract:

In this report, unlike the most previous investigations for wave-induced soil response, a simple analytical model for the random wave-induced soil response is established for an unsaturated seabed of an infinite or finite thickness. Two different wave spectra, B-M and JONSWAP spectra, are considered in the new model. The influence of random wave loading on the soil response is investigated by comparing with the corresponding representative regular wave results through a parametric study, which includes the effect of the degree of saturation, soil permeability, wave height, wave period and seabed thickness. The maximum liquefaction depth under the random waves is also examined. The difference on the soil response under the two random wave types, B-M and JONSWAP frequency spectra, is also discussed in the present work.

Keywords:

Soil response; Seabed liquefaction; pore pressure; effective normal stress; shear stress; random wave; regular wave

Copyright Notice

Department of Civil Engineering, Research Report R864
Random Wave-Induced Seabed Response

h.liu@civil.usdy.edu.au d.jeng@civil.usyd.edu.au

ISSN 1833-2781

Published by:
School of Civil Engineering
The University of Sydney
Sydney NSW 2006
AUSTRALIA

April 2006

This report and other Research Reports published by The School of Civil Engineering are available on the Internet:

http://www.civil.usyd.edu.au

Table of Contents

List of Tables

List of Figures

NOTATIONS

C_i^m	coefficients in the analytical solutions
E	Young's modulus
F_H	random wave high frequency
F_L	random wave low frequency
G	shear modulus
$H_{1/3}$	highest one-third wave (or significant wave) height
H_r	representative regular wave height
K'	apparent bulk modulus of the pore water
K_0	coefficient of earth pressure at rest
K_w	true bulk modulus of elasticity of water
K_x	horizontal soil permeability
K_z	vertical soil permeability
L_r	representative regular wave length
N	total number of the recorded data
N_{wave}	total individual wave number of one wave record
P_{w0}	absolute pore-water pressure
$R(\tau)$	auto-correlation function
$S(f)$	frequency spectrum
S_r	degree of soil saturation
$\overline{T}$	mean wave period
$T_{1/3}$	highest one-third wave (or significant wave) period
T_p	wave period corresponding to the frequency at the spectral peak
T_r	representative regular wave period
T_{tot}	simulated random wave recording length
Z_L	maximum liquefaction depth
a_i	*i*-th component wave amplitude
d	water depth
$\tilde{f}_i$	*i*-th representative frequency
f_N	Nyquist frequency or folding frequency

f_p	spectral peak frequency
g	gravitational acceleration
h	finite soil depth
k_i	*i*-th component wave number
m_n	the *n*-th spectral moment
n'	soil porosity
p	wave-induced pore pressure
p_b	seabed pore pressure amplitude
t	time
u	horizontal soil displacement
w	vertical soil displacement
x	horizontal axis
z	vertical axis
β	compressibility of the pore fluid
δ_m	coefficient in the analytical solutions
γ	peak enhancement factor for JONSWAP spectrum
γ_s	unit weight of soil
γ_w	unit weight of the pore-water
ε	volume strain of soil skeleton
ε_i	random initial phase angle
η	water surface elevation
λ_m	coefficient in the analytical solutions
μ	omitting energy percentage beyond considered frequency range; Poisson's ratio
σ'_x	horizontal effective normal stress in soil skeleton
σ'_z	vertical effective normal stress in soil skeleton
τ_{xz}	shear stress in soil skeleton
ω_N	Nyquist angular frequency or folding angular frequency
Δt	time interval of a record

1 INTRODUCTION

The evaluation of the wave-induced soil response is particularly important for many coastal structures and offshore installations, such as pipelines, marine platforms and breakwaters. When water waves propagate over a porous seabed, the dynamic pressure on the sea floor fluctuates with the passing waves. Such fluctuations induce variations of the pore pressure and effective stress within the marine sediments, and cause the deformation or even failure of the seabed skeleton. Numerous coastal structures have been damaged by the wave-induced seabed instability such as liquefaction (Sumer and Fredsøe, 2002). Moreover, the wave-induced pore pressure within marine sediments is a key factor to estimate the seepage exchange between the sea water body and bottom sediments, which dominates the mass transfer rate between the sediment and seawater (Oldham and Laery, 1999), and is important for studying the water pollution in coastal areas.

In the last few decades, numerous studies have been carried out to investigate the wave-induced pore pressure and effective stress within marine sediments using physical or mathematical approaches. As for experimental studies, wave-induced pore pressure measurements inside the sand bed were conducted in the wave tank experiments using various methods, i.e., pressure trappings in Sleath (1970) or pore-water pressure transducers in Yamamoto et al. (1978) and Tsui and Helfrich (1983).

Accompanying with the experimental efforts, numerous theoretical investigations, including analytical and numerical approaches, were carried out to examine the soil response based on different assumptions of relative rigidity of pore fluid and soil skeleton, such as soil thickness (infinite or finite depth), soil permeability (hydraulically isotropic or anisotropic) and pore fluid compressibility related to the degree of saturation. Among these, Madsen (1978) and Yamamoto et al. (1978) employed Biot's consolidation equations (Biot, 1941) for soil responses in a plane poroelastic sea bed and obtained analytical solutions. Their final governing equation is a linear differential equation of the sixth order. Okusa (1985) further developed the analytical solutions for soil response with a linear differential equation of only forth order which has a clear physical meaning. Mei and Foda (1981) applied a boundary layer near the seabed surface and derived the soil response both in the boundary layer and outer region. All the aforementioned approaches are for soil response of

infinite thickness. Moshagen and Tørum (1975) and Jeng (1997) proposed the analytical solutions with a finite depth. As for analytical solutions, the main difficulties for finite soil thickness have been summarized in Jeng and Hsu (1996). Incidentally, Thomas (1995) and Cheng et al. (2001) applied numerical methods to solve the soil response inside the seabed. However, all the previous works are based on the regular wave theory as the first approximation, even though the random waves always occur in the realistic ocean environments.

To date, only a few studies have been carried out to consider the variations on the soil responses inside the marine sediments under random wave loadings. Sumer et al. (1999) performed experimental tests to investigate the effect of irregular wave on soil response, and they found the process of build-up of pore pressure in irregular waves occurs in much the same way as in the case of the regular wave. Later, Wang et al. (2005) developed a finite element model to numerically examine the effects of random waves on the wave-induced pore pressure and effective stress based on the dynamic model of Zienkiewicz and Chang (1980).

In this report, based on the framework proposed by Jeng (1997), we will establish a semi-analytical solution for the random wave-induced soil response. Two typical frequency spectra, B-M spectrum and JONSWAP spectrum, will be utilized to generate the random waves. The present investigation is a twofold work: the soil response of infinite thickness and that of finite thickness. The objective of this study is to investigate the random wave-induced soil response in the marine sediments. A set of numerical calculations for pore pressure, effective normal stresses and shear stress will be carried out and compared with the representative regular wave results to demonstrate the effect of wave randomness. Influence of various soil and wave parameters as well as the effect of porous seabed thickness on the random wave-induced soil response will also be considered in this report. Finally, random wave-induced maximum liquefaction depth will be investigated and compared with the corresponding regular wave results.

This report is outlined as the follows: section 2 presents the random wave theory in which the present research domain, random wave generation and validation, statistic features of the simulated random waves together with the representative regular

wave characteristics are discussed in detail. Then, Section 3 specifies the soil response boundary value problem as well as the corresponding boundary conditions. After that, the semi-analytical solutions for random wave-induced soil response of an infinite or finite soil thickness are obtained in Section 4. Knowing these, discussions and analyses are carried out in Section 5. Finally, conclusions from the present study are drawn in Section 6. The corresponding Fortran program code together with the relevant user manual is attached as Appendix.

2 RANDOM WAVES

2.1 Research Domain

In this study, we consider a series of random waves propagating over a porous seafloor with an infinite thickness or a finite thickness (h) above a rigid impermeable bottom, as shown in Fig. 1. In realistic environment, random waves instead of regular linear wave loadings always occur. Such random waves characterizing with irregular water surface elevation introduce the relevant change on the wave dynamic pressure acting at the seabed, which further induce the variation of pore water pressure and effective stresses inside the marine sediments.

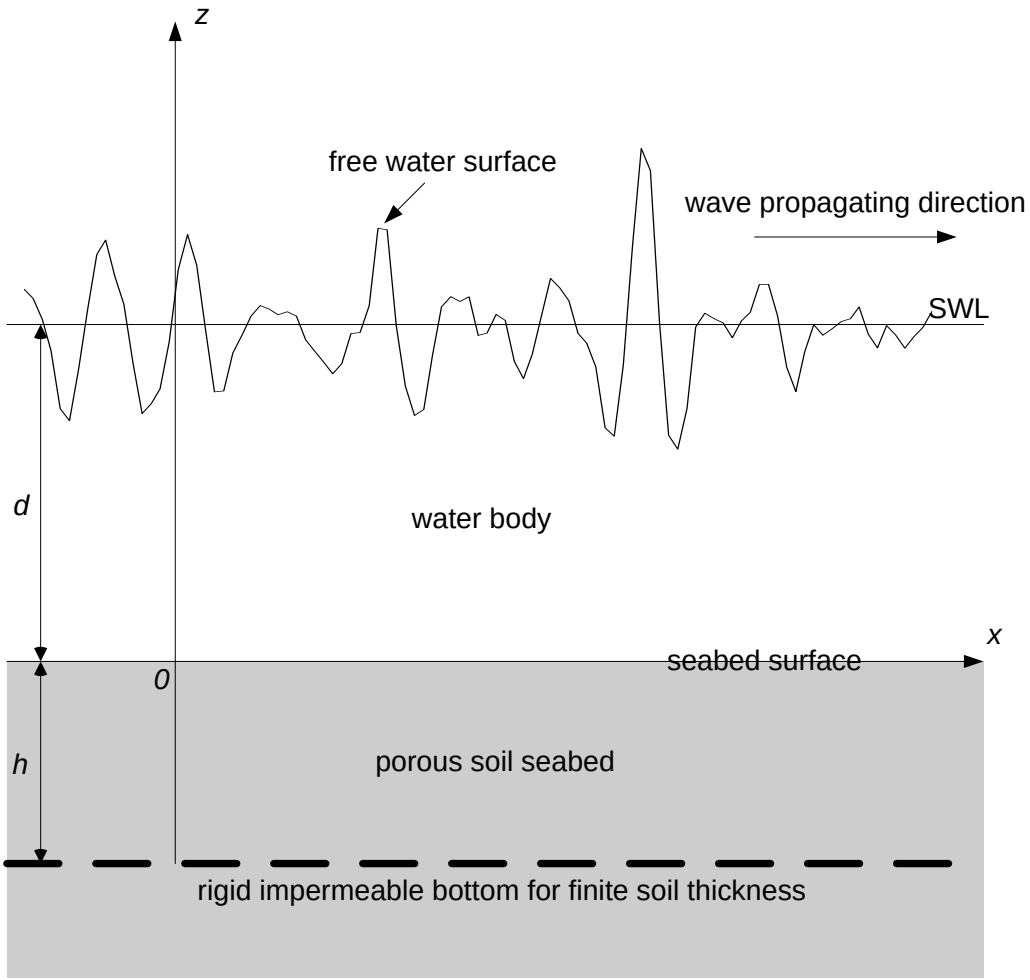

Fig. 1 Definition sketch of random wave propagating over a porous seabed.

Herein, we consider the flow is two-dimensional and assume the random waves with still water level (SWL) located at $z = d$ are traveling along the positive *x*-direction, and assume the vertical *z*-axis is upward from the surface of the seabed (water-soil

interface, $z = 0$) as illustrated in Fig. 1. A porous seabed with a soil thickness h is located between the seabed surface and a rigid impermeable bottom for a finite soil depth.

2.2 Random Wave Generation

The profile of random sea waves can be regarded as a stationarity stochastic process, which follows the Gaussian (normal) distribution. Such process satisfies the property of ergodicity. When we consider the profile of random sea waves, following the mathematical representations of Longuet-Higgins (1957), the wave profile or the water surface elevation $\eta(x,t)$ can be represented by,

$$\eta(x,t) = \sum_{i=1}^{\infty} a_i \cos\left(k_i x - 2\pi \tilde{f}_i t + \varepsilon_i\right) \approx \sum_{i=1}^{M} a_i \cos\left(k_i x - 2\pi \tilde{f}_i t + \varepsilon_i\right) \tag{1}$$

with M being a sufficiently large number. In Eq. (1), a_i denotes the amplitude of the component wave in the *i*-th frequency, $\tilde{f}_i$ is the *i*-th representative frequency, which is evenly distributed in the range of (f_{i-1}, f_i), and ε_i is a random initial phase angle and equally distributed in the range of (0, 2π). In this equation, wave number of the *i*-th component, k_i, can be determined from the dispersion relationship after knowing the corresponding representative frequency $\tilde{f}_i$ and water depth d,

$$\left(2\pi \tilde{f}_i\right)^2 = g k_i \tanh k_i d\,, \tag{2}$$

in which g denotes the gravitational acceleration. The component wave amplitude a_i is determined from a given function of the frequency spectrum $S(f)$ by,

$$a_i = \sqrt{2S(\hat{f}_i)\Delta f_i}\,,\ \hat{f}_i = \left(f_i + f_{i-1}\right)/2, \Delta f_i = f_i - f_{i-1}, \tag{3}$$

In this study, two commonly used frequency spectra, B-M spectrum and JONSWAP spectrum, are adopted for further discussions. Here, we summarized these two standard frequency spectral density functions as: (Goda, 2000)

(a) B-M spectrum,

$$S(f) = 0.257 H_{1/3}^2 T_{1/3}^{-4} f^{-5} \exp[-1.03(T_{1/3} f)^{-4}], \tag{4}$$

where $H_{1/3}$ and $T_{1/3}$ denote the highest one-third wave (or significant wave) height and the relevant wave period respectively.

(b) JONSWAP spectrum,

$$S(f) = \beta_J H_{1/3}^2 T_P^{-4} f^{-5} \exp[-1.25(T_P f)^{-4}] \gamma^{\exp[-(T_p f - 1)^2 / 2\sigma^2]}, \quad (5)$$

in which,

$$\beta_J = \frac{0.0624}{0.230 + 0.0336\gamma - 0.185(1.9 + \gamma)^{-1}} \left[1.094 - 0.01915 \ln \gamma\right] \quad (6a)$$

$$T_p = \frac{T_{1/3}}{\left[1 - 0.132(\gamma + 0.2)^{-0.559}\right]} \quad (6b)$$

$$\sigma = \begin{cases} \sigma_a : f \le f_p \\ \sigma_b : f \ge f_p \end{cases} \quad (6c)$$

$\gamma = 1 \sim 7$ (mean of 3.3), $\sigma_a = 0.07$, $\sigma_b = 0.09$ (6d)

where T_p represents the wave period corresponding to the frequency f_p at the spectral peak. The JONSWAP spectrum is characterized by the peak enhancement factor γ, which controls the sharpness of the spectral peak.

Several points have to be specified here,

(1) Determine the frequency range of random sea waves

As we know, for random waves, the consisted frequency is varying from 0 Hz to +∞ Hz. In the simulation, we set the frequency range between low frequency F_L and high frequency F_H. This means we neglect certain part of wave energy which is contained by the frequencies beyond this range. Assuming μ percent energy is omitted both in the range of $[0, F_L]$ and $[F_H, +\infty]$ (i.e., $\mu = 0.2\%$ in the simulation), for integrabel spectrums, i.e., B-M spectrum in Eq. (4), we have,

$$F_L = \frac{1}{T_{1/3}} \left(-\frac{1.03}{\ln \mu} \right)^{1/4} \quad (7a)$$

$$F_L = \frac{1}{T_{1/3}} \left(-\frac{1.03}{\ln(1-\mu)} \right)^{1/4} \quad (7b)$$

For JONSWAP spectrum in Eq. (5), it is not so easy to be integrated. Consider the wave energy is mainly concentrated around the peak frequency, we assume (such approach also appears in Goda, 2000),

$$F_L = 0, \qquad F_H = 5 f_p \tag{8}$$

where f_p can be determined from Eq. (6b).

(2) Separate the frequency range $[f_L, f_H]$

Two methods can be applied: equally separating the frequency and equally separating the energy. In the program, equally separating the frequency is utilized, which assumes the frequency is equally divided in the range $[f_L, f_H]$,

$$\Delta f = \frac{f_H - f_L}{M} \tag{9}$$

Hence, the whole frequency domain is equally separated as $[f_L, f_L + \Delta f]$, $[f_L + \Delta f, f_L + 2\Delta f] \ldots [f_H - \Delta f, f_H]$. The *i*-th representative frequency, $\tilde{f}_i$, is evenly distributed in the range of $[f_{i-1}, f_i]$ and determined through a random number.

Using Eq. (3), the corresponding *i*-th component wave amplitude a_i can be determined. Hence, the time history of random wave surface elevations can be obtained from Eq. (1).

2.3 Random Wave Simulation

To generate the random waves with aforementioned frequency spectra, the whole range of wave frequency is evenly separated within the specified range of $[f_L, f_H]$, where most of the wave energy is located as specified in the previous context. In this study, we assume the simulated random waves consist of 100 linear wave components, i.e., $M = 100$. Goda (2000) mentioned that in field observation, to keep the sampling variability of the characteristic wave heights and periods below an acceptable level, a recording length of about 20 min is employed as a compromise between the requirements of wanting low sampling variability and having a stationary, which includes about 100 consecutive waves. The data sampling interval of 1/10 to 1/20 of the significant wave period is recommended.

Figure 2 illustrates the time history of the water surface elevation η at the fixed point $x = 0$. The upper panel demonstrates the result using B-M spectrum while the lower one is for the result of JONSWAP spectrum. Water surface irregularity caused by the wave randomness can be clearly observed from this figure with water surface elevation fluctuates around the zero level. In the numerical calculation, the significant wave period $T_{1/3}$ and wave height $H_{1/3}$ are assumed to be 10 s and 6 m respectively, and the water depth is 25 m. Taking into account the statistical principle for record data length and time interval of data sampling mentioned above, time interval $\Delta t = 1$ s and a recording length $T_{tot} = 1000$ s are adopted in the present study.

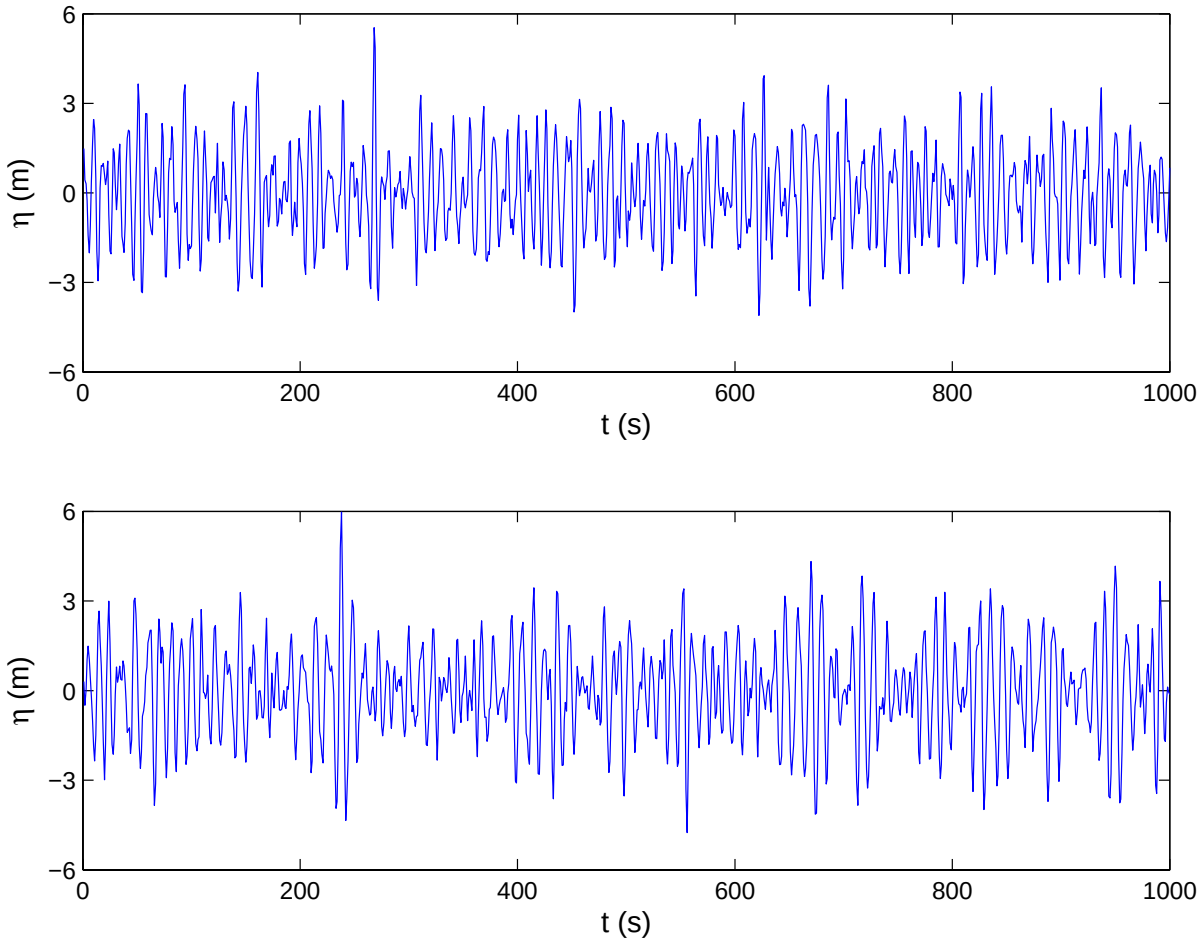

Fig. 2 Time history of simulated random wave profiles using different frequency spectra: B-M Spectrum (upper panel), JONSWAP Spectrum (lower panel).

2.4 Random Wave Validation

After generating the random waves, validation of the simulated random wave profile is needed to assure the precision and efficiency of the numerical simulation. This is

conducted by comparing the simulated or predicted frequency spectrum with the target frequency spectrum presented in Eqs. (4) and (5) after considering that all the typical random wave characteristics, such as significant wave height and period, can be determined by the frequency spectrum (Goda, 2000).

After knowing the water surface elevation $\eta(x,t)$ distribution from Eq. (1), there are two methods which can be applied to determine the simulated (predicted) spectrum: auto-correlation method and FFT method. In this study, the auto-correlation method is utilized. Assuming the profile of random sea wave is a stationarity stochastic process, for one wave recording surface elevation data, η_1, η_2, …, η_N, the auto-correlation function is estimated as,

$$R(\tau) = \frac{1}{N-\nu}\sum_{n=1}^{N-\nu}\eta_{n+\nu}\eta_n, \qquad \nu = 0,1,2,...,m \tag{10}$$

Assuming the data sampling interval is Δt, then,

$$R(\tau) = R(\nu\Delta t) = \frac{1}{N-\nu}\sum_{n=1}^{N-\nu}\eta(t_n+\nu\Delta t)\eta(t_n) \qquad \tau = \nu\Delta t,\ \nu = 0,1,2,...,m \tag{11}$$

We can have $m+1$ values of correlation function $R(\tau)$ which are equally distributed at $\tau = 0, \Delta t, 2\Delta t, ..., m\Delta t$. The frequency spectrum $S(\omega)$ or $S(f)$ can be estimated by,

$$S(\omega) = \frac{2}{\pi}\int_0^\infty R(\tau)e^{-i\omega t}dt$$
$$S(f) = 4\int_0^\infty R(\tau)e^{-i2\pi ft}dt \tag{12}$$

Considering the effect of Nyquist frequency or folding frequency f_N,

$$f_N = \frac{\omega_N}{2\pi} = \frac{1}{2\Delta t} \tag{13}$$

the predicted spectrum is distributed in the range of $[0, f_N]$. Assuming the equally distributed $m+1$ values of frequency $f_0 = 0$, f_1, f_2 … $f_m = f_N$, then for one specified frequency f_n,

$$f_n = n\Delta f = \frac{n}{m}\frac{1}{2\Delta t} \qquad \omega_n = 2\pi f_n \tag{14}$$

What we are concerning now is to get the frequency spectrum values at these specified frequencies using Eq.(12). Hence, the spectrum at a certain frequency f_n, $S'(f_n)$, can be estimated as,

$$S'(f_n) = \frac{2}{\pi}\sum_{\tau=0}^{m\Delta t} R(\tau)\cos\omega_n \tau d\tau = \frac{2}{\pi}\sum_{\nu=0}^{m} R(\nu\Delta t)\cos(\omega_n \nu\Delta t)\Delta t \tag{15}$$

Using trapezoidal formula for integration, we have,

$$S'(f_n) = \frac{2}{\pi}\left(\frac{1}{2}R(0) + \sum_{\nu=1}^{m-1} R(\nu\Delta t)\cos(\omega_n \nu\Delta t) + \frac{1}{2}R(m\Delta t)\cos(\omega_n m\Delta t)\right)\Delta t \tag{16}$$
$$n = 0,1,2,...,m$$

Substituting Eq. (14) into (16) we can obtain the frequency spectrum as,

$$S'(f_n) = \frac{2\Delta t}{\pi}\left(\frac{1}{2}R(0) + \sum_{\nu=1}^{m-1} R(\nu\Delta t)\cos\frac{\pi\nu n}{m} + \frac{1}{2}R(m\Delta t)\cos\pi n\right) \tag{17}$$
$$n = 0,1,2,...,m$$

Using the aforementioned method, the predicted spectrum $S'(f_n)$ is not completely precise, and the shape of the spectrum curve has lots of fluctuation. To improve the simulation, we introduce the weight functions. After multiplying the auto-correlation function $R(\tau)$, we can finally obtain the smoothed spectrum distribution $S(f_n)$. Such weight functions have various forms, in this study we apply the Hamming Window as,

$$S(f_n) = 0.23S'(f_{n-1}) + 0.54S'(f_n) + 0.23S'(f_{n+1}) \tag{18}$$

At two lateral boundaries,

$$S(f_0) = 0.54S'(f_0) + 0.46S'(f_1) \tag{19a}$$

$$S(f_n) = 0.46S'(f_{n-1}) + 0.54S'(f_n) \tag{19b}$$

Other frequently utilized approaches include Hanning Window, which has the following expression,

$$S(f_n) = 0.25S'(f_{n-1}) + 0.5S'(f_n) + 0.25S'(f_{n+1}) \tag{20}$$

At two lateral boundaries,

$$S(f_0) = 0.5S'(f_0) + 0.5S'(f_1) \tag{21a}$$

$$S(f_n) = 0.5S'(f_{n-1}) + 0.5S'(f_n) \tag{21b}$$

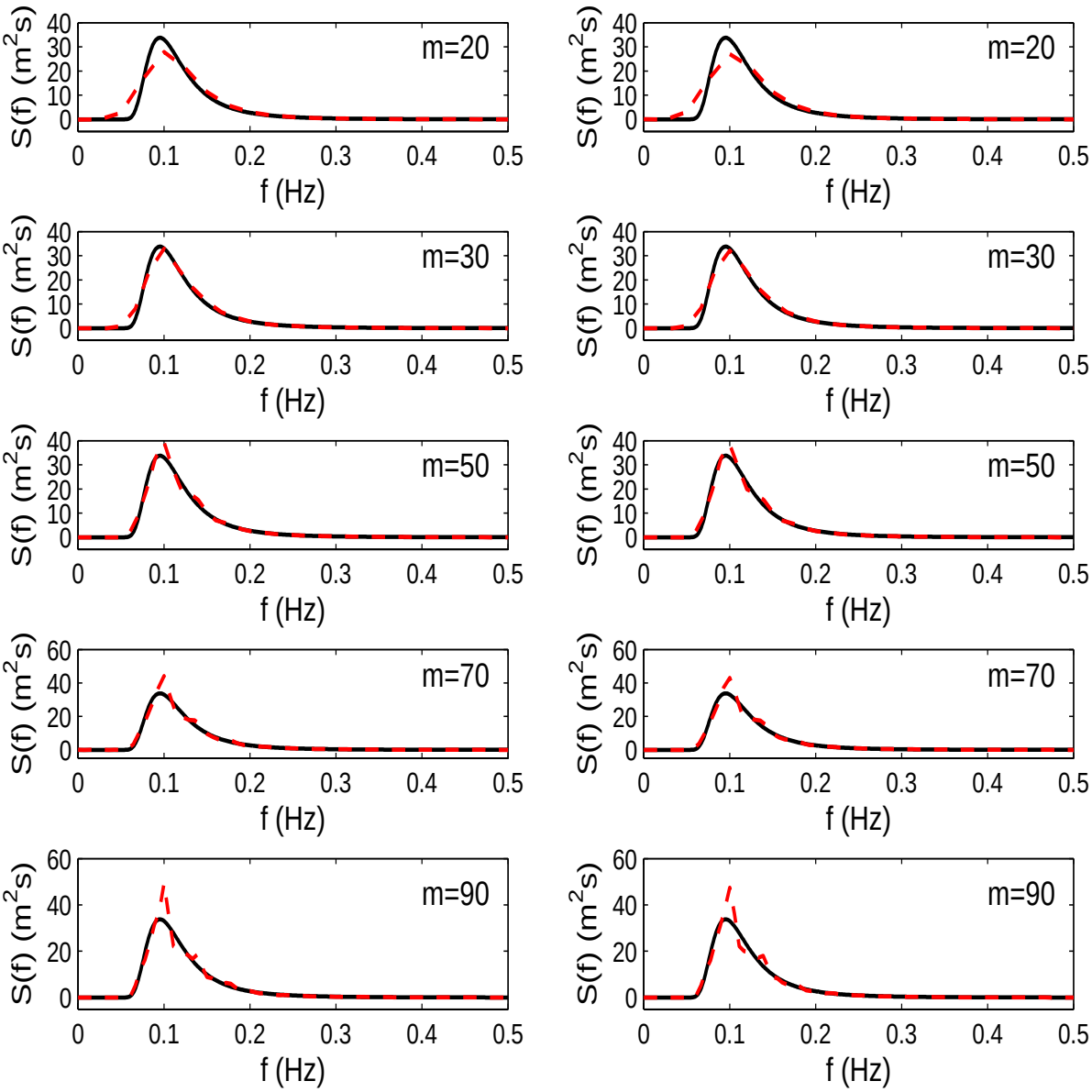

Fig. 3 Comparison of the predicted spectrum (dashed lines) and target spectrum (solid lines) for B-M Spectrum using Hamming Window (left panels) and Hanning Window (right panels) for different m values varying from 20 to 90.

Figure 3 illustrates the comparison of the predicted spectrum (dashed lines) and target spectrum (solid lines) for B-M Spectrum using Hamming Window (left panels) and Hanning Window (right panels) for different m values varying from 20 to 90. Considering that the sampling interval is 1 s for the simulated wave profile, the highest frequency to which the spectrum can be estimated is 0.5 Hz. From this figure, we can see that with the increasing of m value, the predicted spectrum peak values increase while the fluctuation of the predicted spectrum profiles also increase, especially after the spectral peak frequency, f_p. Nevertheless, with the decreasing of m value, the predicted spectrum peak values decrease while the predicted spectrum profiles become smooth (further decreasing m will induce the incontinuity considering that m represents the total number of the predicted frequency and relevant spectrum value). There is no clear difference on the predicted spectrum profiles between the Hamming Window and the Hanning Window.

Figure 4 presents the corresponding results for JONSWAP Spectrum. In this figure, only the results using Hamming Window are demonstrated. From this figure we can see, the same phenomenon for predicted spectrum profiles can be observed: small value of m underestimates the peak spectrum and large m value causes the fluctuation of the spectrum distribution. Yu (1992) suggested the value of m should be around $N/(15 \sim 20)$, in which N is the total number of the recorded data.

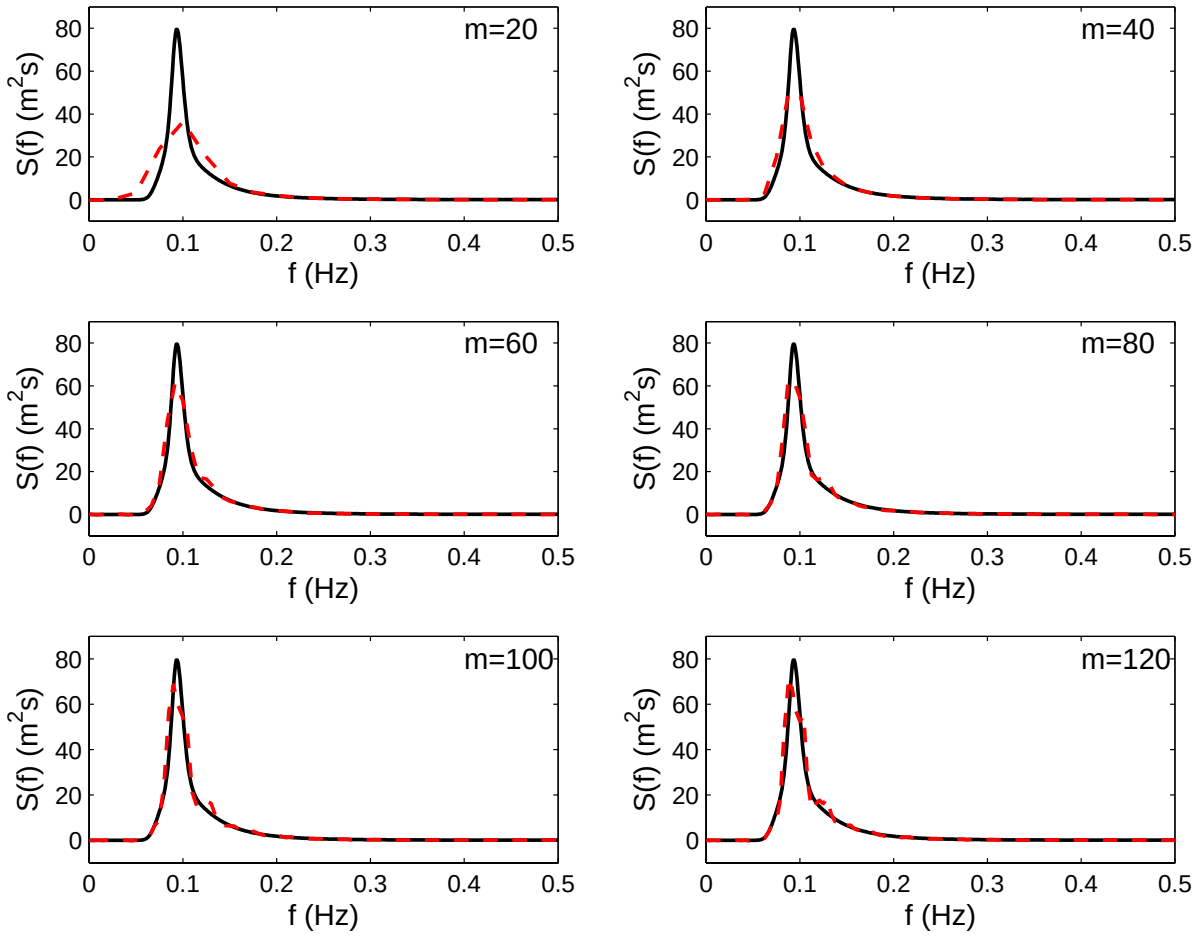

Fig. 4 Comparison of the predicted spectrum (dashed lines) and target spectrum (solid lines) for JONSWAP Spectrum using Hamming Window for different m values varying from 20 to 120.

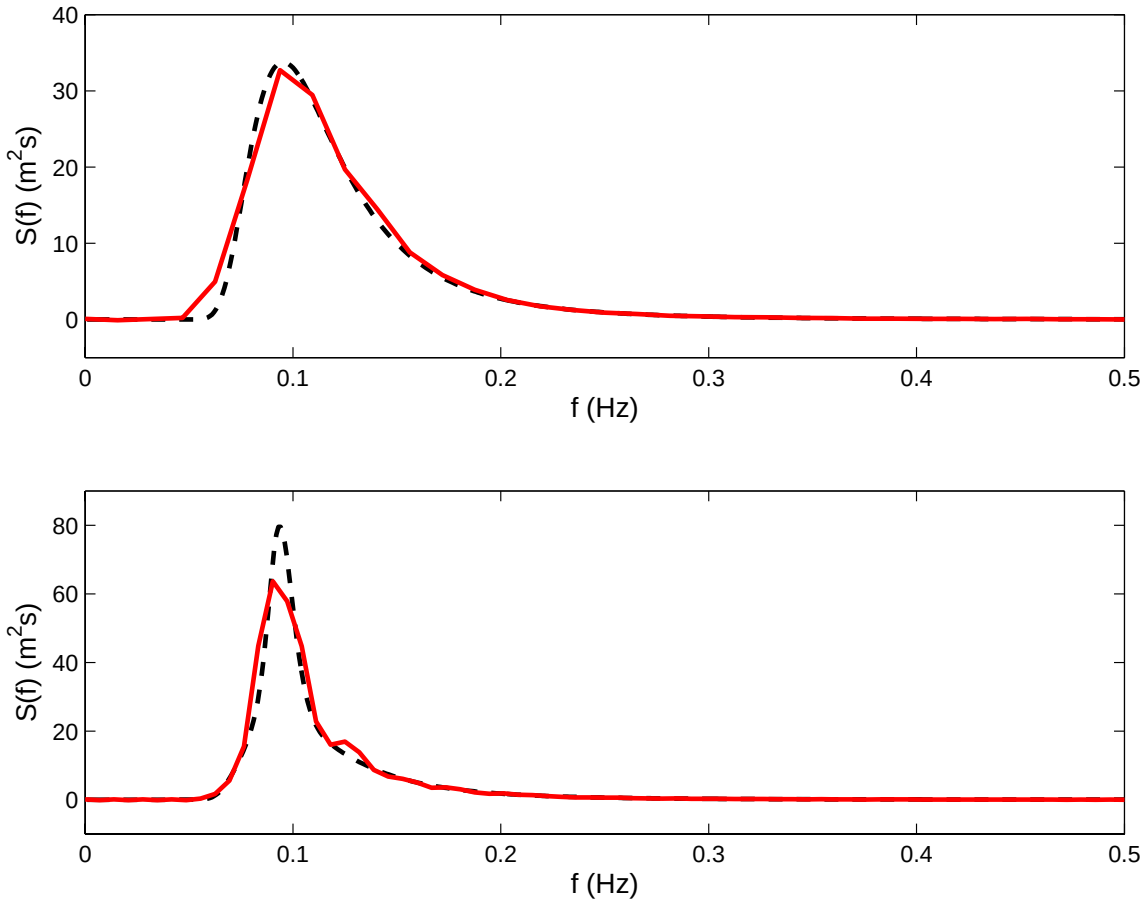

Fig. 5 Comparison of predicted spectrum (solid lines) and target spectrum (dashed lines): B-M Spectrum (upper panel), JONSWAP Spectrum (lower panel).

Figure 5 presents the comparison between the target and predicted spectra for both B-M spectrum and JONSWAP spectrum. For these two frequency spectra, the wave energy concentrates around the peak frequency f_p, which is almost equal to the frequency corresponding to the significant wave period, i.e., $f_{1/3} = 1/T_{1/3} = 0.1$ Hz (Strictly speaking, f_p is a little bit smaller than $f_{1/3}$ as we can see from Eq. 6b). Both the profile and magnitude of the target spectrum can be captured by the present predicted spectrum although there exists some underestimation, especially for the JONSWAP spectrum case around the maximum spectra value. As for the JONSWAP spectrum with peak enhancement factor $\gamma = 3.3$, the peak spectra value is about 2.2 times of the B-M spectrum result. As a whole, Figure 5 demonstrates that the simulation of random wave is effective and can be used for the analysis of the dynamics response of seabed.

2.5 Statistic Features of the Simulated Random Waves

After the simulation of the time history of random wave surface elevation at a fixed point, $\eta(t)$, we can count the statistic features of the random waves, such as how many individual waves in one wave record, the highest one-*n*th wave height and relevant wave period ($n=1$ for mean wave value; $n=3$ for highest one-third wave value or significant wave value; $n=10$ for one-tenth wave value; $n=N_{wave}$ for highest wave value in which N_{wave} is the total individual wave number of one wave record).

Before doing the statistic analysis, we need to correct for mean water level. A simple procedure to determine the mean water level is to use the arithmetic mean of all the data points. After that, we can first count the total number of individual waves in one record. In this study, we use the definition of zero-upcrossing method to do analysis. Zero-upcrossing of the wave profile is detected through the following criteria (Goda, 2000),

$$\eta_i \eta_{i+1} < 0 \qquad and \qquad \eta_{i+1} > 0 \tag{22}$$

where η_i denotes the *i*-th data point of the surface elevation after correction of thee mean water level. Applying the zero-up-crossing method for defining individual waves, the simulated recording length includes 120 wave cycles using the B-M spectrum or 117 waves in case that JONSWAP spectrum is utilized.

In order to determine the zero-upcrossing wave height, the highest point on the surface elevation must be searched for in the time interval between two successive zero-upcrossing points. Once this point is obtained among the sampled points, say, η_i, and then the true maximum elevation $\eta_{\max}$ between two zero-upcrossoing points can be estimated by fitting a parabolic curve to the three conjoint points η_{i-1}, η_i and η_{i+1} in order to eliminate the underestimation. The formula for a parabolic fitting is,

$$\eta_{\max} = C - B^2 / 4A \tag{23}$$

where,

$$A = \frac{1}{2}\left(\eta_{i-1} - 2\eta_i + \eta_{i+1}\right), \qquad B = \frac{1}{2}\left(\eta_{i+1} - \eta_{i-1}\right), \qquad C = \eta_i \tag{24}$$

The lowest surface elevation $\eta_{\min}$ is obtained by a similar process, and the wave height is calculated as the sum of the absolute values of $\eta_{\max}$ and $\eta_{\min}$.

After knowing the total number of individual waves and specifying the beginning/ending time and wave heights of every individual wave, we can obtain the statistic features of the random waves according to their definitions. Table 1 lists such statistic features of the simulated B-M type random waves and JONSWAP type random waves. From this table we can see, the simulated statistic features for JONSWAP spectrum present better estimation considering that the target significant wave height and period are 6 m and 10 s respectively. As for the results of B-M spectrum, the simulated features somewhat underestimate the target values.

Table 1 Statistic features of the simulated random waves

	N_{wave}	Mean values		1/3 highest values		1/10 highest values		the highest values	
		Wave height (m)	Wave period (s)	Wave height (m)	Wave period (s)	Wave height (m)	Wave period (s)	Wave height (m)	Wave period (s)
B-M Spectrum	120	3.40	8.26	5.62	9.19	6.68	8.79	9.37	7.67
JONSWAP Spectrum	117	3.59	8.50	6.00	9.91	7.52	10.06	10.44	9.90

2.6 Representative Regular Wave

Most of the previous studies focus on the wave-induced soil response under the linear regular wave loading as specified in the previous context. Therefore, it is interesting to investigate the various soil responses under the random waves and try to find the difference between regular and random wave loadings.

To do comparison with regular wave-induced soil response, how to define the suitable representative regular wave parameters (i.e., regular wave height and wave period) in case of considered random wave characteristics is needed. As a first

thinking, we may apply the significant wave height and period ($H_{1/3}$, $T_{1/3}$) as the representative regular wave parameters. However, this means a regular wave with relative large wave height and longer wave period after considering the random wave characteristics. Sumer et al. (1999), from their irregular wave experimental measurement, found that the combination of representative wave height $H_r = H_{1/3}/\sqrt{2}$ and wave period $T_r = \overline{T}$ provide the best comparison with the regular wave results, where H_r can be interpreted as the equivalent sinusoidal wave height of the irregular waves, and T_r represents the mean zero-upcrossing period of a random wave record, which can be determined from the frequency spectra $S(f)$ by (Goda, 2000)

$$T_r = \overline{T} = \sqrt{m_0 / m_2} \tag{25a}$$

$$m_n = \int_0^\infty f^n S(f) df, \quad n = 0,2 \tag{25b}$$

where m_n is the *n*-th spectral moment. Applying the random wave characteristics used in previous examples, for B-M spectrum, the corresponding representative regular wave height and period are $H_r = 4.24$ m and $T_r = 7.64$ s respectively (hence representative wavelength $L_r = 86.27$ m); for JONSWAP spectrum, these two are $H_r = 4.24$ m and $T_r = 8.48$ s respectively with wavelength $L_r = 102.29$ m.

Using these approach to determine the representative regular wave characteristics, both H_r and T_r are smaller than the corresponding significant values, say, $H_{1/3}$ and $T_{1/3}$. Another thing need to be pointed out is that taking Table 1 into account, the simulated or predicted mean zero-upcrossing wave period (8.26 s) of B-M spectrum somewhat overestimates the target value (7.64 s). Nevertheless, simulation for JONSWAP spectrum provides much better prediction after comparing with the theoretical value.

3 WAVE-INDUCED SOIL RESPONSE

3.1 Governing Equations

The proposed model is based on the physically consistent, consolidation theory developed by Biot (1941), which is generally accepted as the one to control the flow of compressible pore fluid inside a compressible porous medium. For a two-dimensional problem, and considering the porous bed as hydraulically anisotropic with permeabilities K_x and K_z in the horizontal and vertical directions respectively, the governing equation can be expressed as

$$\frac{K_x}{K_z}\frac{\partial^2 p}{\partial x^2}+\frac{\partial^2 p}{\partial z^2}-\frac{\gamma_w n'\beta}{K_z}\frac{\partial p}{\partial t}=\frac{\gamma_w}{K_z}\frac{\partial \varepsilon}{\partial t} \tag{26}$$

where p is the wave-induced pore pressure, γ_w is the unit weight of the pore-water, n' is the soil porosity and ε is the volume strain defined by

$$\varepsilon=\frac{\partial u}{\partial x}+\frac{\partial w}{\partial z} \tag{27}$$

where u and w are the soil displacement in the *x*- and *z*-directions respectively.

In (26), the compressibility of the pore fluid β is related to the apparent bulk modulus of the pore water K', which is a function of the true bulk modulus of elasticity of water K_w, the degree of saturation S_r and absolute pore-water pressure P_{w0}

$$\beta=\frac{1}{K'}=\frac{1}{K_w}+\frac{1-S_r}{P_{w0}} \tag{28}$$

In case that pore-water is absolutely air-free, i.e., fully saturated, then $\beta=1/K_w\approx 0$ since $S_r=1$ and K_w has a very large value (which may be taken as 1.9×10^9 N/m^2 according to Yamamoto et al., 1978).

The equations for overall equilibrium in a poro-elastic medium, relating to the effective stresses and pore pressure, are given by

$$\frac{\partial \sigma_x'}{\partial x}+\frac{\partial \tau_{xz}}{\partial z}=\frac{\partial p}{\partial x} \tag{29a}$$

$$\frac{\partial \tau_{xz}}{\partial x}+\frac{\partial \sigma_z'}{\partial z}=\frac{\partial p}{\partial z} \tag{29b}$$

in which σ_x' and σ_z' are the horizontal and vertical effective normal stress respectively, and τ_{xz} denotes the shear stress.

Based on the generalized Hooke's law, the relationships between elastic incremental effective stresses and soil displacements are given by

$$\sigma_x' = 2G\left[\frac{\partial u}{\partial x} + \frac{\mu}{1-2\mu}\varepsilon\right] \tag{30a}$$

$$\sigma_z' = 2G\left[\frac{\partial w}{\partial z} + \frac{\mu}{1-2\mu}\varepsilon\right] \tag{30b}$$

$$\tau_{xz} = G\left[\frac{\partial u}{\partial z} + \frac{\partial w}{\partial x}\right] \tag{30c}$$

where the shear modulus G is related to Young's modulus E by the Poisson's ratio μ in the form of $E/2(1+\mu)$.

Substituting (30) into (29) yields the equations of force equilibrium

$$G\nabla^2 u + \frac{G}{(1-2\mu)}\frac{\partial \varepsilon}{\partial x} = \frac{\partial p}{\partial x} \tag{31a}$$

$$G\nabla^2 w + \frac{G}{(1-2\mu)}\frac{\partial \varepsilon}{\partial z} = \frac{\partial p}{\partial z} \tag{31b}$$

in the horizontal and vertical directions respectively.

Equations (26) and (31) form a system of three partial differential equations in terms of three unknown variables, p, u and w. For a homogeneous soil matrix, mathematical expressions for the water-induced soil response can be derived with appropriate boundary conditions.

3.2 Boundary Conditions

To solve the three coupled partial differential equations, three independent conditions are needed at each boundary.

In case of infinite soil thickness under random wave loadings, at large depth, it is obvious that no soil displacement will be experienced, and also no porewater pressure will develop. Therefore

$$u = w = p = 0 \quad \text{at } z \to -\infty \tag{32}$$

In case of finite soil thickness, the soil particles rest on the impermeable rigid bottom and no soil displacement will be experienced

$$u = w = 0 \quad \text{at } z = -h \tag{33}$$

At the rigid bottom, no vertical flow or velocity occurs. Considering that the flow velocity is related to the pressure gradient through Darcy's law, the following pressure condition is obtained

$$\frac{\partial p}{\partial z} = 0 \quad \text{at } z = -h \tag{34}$$

At the seabed surface $(z = 0)$, it is commonly accepted that both vertical effective stress and shear stress vanish, i.e.

$$\sigma_z' = \tau_{xz} = 0 \quad \text{at } z = 0 \tag{35}$$

and the pore pressure is equal to the wave-induced pressure at the seabed surface. Under the random wave conditions, the wave dynamic pressure along the seafloor is expressed as the superposition of a large number of linear regular wave results at the seabed

$$p_b(x,t) = \sum_{i=1}^{M} p_b^{(i)} \cos(k_i x - 2\pi \tilde{f}_i t + \varepsilon_i) \tag{36a}$$

$$p_b^{(i)} = \frac{\gamma_w a_i}{\cosh k_i d} = \frac{\gamma_w \sqrt{2S(\hat{f}_i)\Delta f_i}}{\cosh k_i d} \quad \text{at } z = 0 \tag{36b}$$

4 ANALYTICAL SOLUTIONS

The boundary value problem specified in Section 3, describing the wave-seabed interaction, can be solved based on the governing equations (26) and (31) with suitable boundary conditions, i.e., (32), (35) and (36) for infinite soil thickness; (33)-(36) for finite soil thickness. The analytical solution for the wave-induced pore pressure p and soil displacements u and w can first be obtained, from which various effective stresses can be found from (30). A series of closed-form analytical solutions for soil response in a porous seabed under the linear regular wave loading have been developed by Jeng (1997).

4.1 An Infinite Seabed

Following the framework proposed by Jeng (1997) for regular waves and for the present two-dimensional problem, the random wave-induced pore pressure and displacements for infinite soil thickness can be written as

$$p = \mathbf{Re}\left\{\sum_{m=1}^{M}\frac{p_b^{(m)}}{1-2\mu}\left[\left(1-2\mu-\lambda_m\right)C_1^m e^{k_m z} + \frac{\delta_m^2-k_m^2}{k_m}\left(1-\mu\right)C_2^m e^{\delta_m z}\right]e^{i(k_m x-\omega_m t+\varepsilon_m)}\right\} \tag{37}$$

$$u = \mathbf{Re}\left\{\sum_{m=1}^{M}\frac{ip_b^{(m)}}{2G}\left[\left(C_0^m + C_1^m z\right)e^{k_m z} + C_2^m e^{\delta_m z}\right]e^{i(k_m x-\omega_m t+\varepsilon_m)}\right\} \tag{38}$$

$$w = \mathbf{Re}\left\{\sum_{m=1}^{M}\frac{p_b^{(m)}}{2G}\left[\left(C_0^m - \frac{1+2\lambda_m}{k_m}C_1^m + C_1^m z\right)e^{k_m z} + \frac{\delta_m}{k_m}C_2^m e^{\delta_m z}\right]e^{i(k_m x-\omega_m t+\varepsilon_m)}\right\} \tag{39}$$

where $\mathbf{Re}\{\ \}$ represents the real part of the function, and $\omega_m = 2\pi\tilde{f}_m$ is the angular frequency of the *m*-th component wave. Coefficients δ_m and λ_m are expressed as

$$\delta_m^2 = k_m^2\frac{K_x}{K_z} - \frac{i\omega_m\gamma_m}{K_z}\left(n'\beta + \frac{1-2\mu}{2G(1-\mu)}\right) \tag{40a}$$

$$\lambda_m = \frac{\left(1-2\mu\right)\left[k_m^2\left(1-\frac{K_x}{K_z}\right) + \frac{i\omega_m\gamma_m n'\beta}{K_z}\right]}{k_m^2\left(1-\frac{K_x}{K_z}\right) + \frac{i\omega_m\gamma_m}{K_z}\left(n'\beta + \frac{1-2\mu}{G}\right)} \tag{40b}$$

Substituting Eqs. (38-39) into Eq. (30), the effective normal stresses σ_x', σ_z' and shear stress τ_{xz} can be determined as

$$\sigma_x' = \mathbf{Re}\left\{-\sum_{m=1}^{M} p_b^{(m)}\left[\left(k_m\left(C_0^m + C_1^m z\right) + \frac{2\mu\lambda_m}{1-2\mu}C_1^m\right)e^{k_m z} + \left(k_m - \frac{\mu(\delta_m^2 - k_m^2)}{k_m(1-2\mu)}C_2^m e^{\delta_m z}\right)\right]e^{i(k_m x - \omega_m t + \varepsilon_m)}\right\} \tag{41}$$

$$\sigma_z' = \mathbf{Re}\left\{\sum_{m=1}^{M} p_b^{(m)}\left[\left(k_m C_0^m + C_1^m k_m z - \frac{2\lambda_m(1-\mu)}{1-2\mu}C_1^m\right)e^{k_m z} + \frac{\delta_m^2(1-\mu) - k_m^2\mu}{k_m(1-2\mu)}C_2^m e^{\delta_m z}\right]e^{i(k_m x - \omega_m t + \varepsilon_m)}\right\} \tag{42}$$

$$\tau_{xz} = \mathbf{Re}\left\{\sum_{m=1}^{M} ip_b^{(m)}\left\{\left[k_m C_0^m + (k_m z - \lambda_m)C_1^m\right]e^{k_m z} + \delta_m C_2^m e^{\delta_m z}\right\}e^{i(k_m x - \omega_m t + \varepsilon_m)}\right\} \tag{43}$$

In the expressions of (37)-(43), the coefficients $C_i^m (i = 0,1,2)$ are obtained by

$$C_0^m = \frac{-\lambda_m\left[\mu(\delta_m - k_m)^2 - \delta_m(\delta_m - 2k_m)\right]}{k_m(\delta_m - k_m)(\delta_m - \delta_m\mu + k_m\mu + k_m\lambda_m)} \tag{44a}$$

$$C_1^m = \frac{\delta_m - \delta_m\mu + k_m\mu}{\delta_m - \delta_m\mu + k_m\mu + k_m\lambda_m} \tag{44b}$$

$$C_2^m = \frac{k_m\lambda_m}{(\delta_m - k_m)(\delta_m - \delta_m\mu + k_m\mu + k_m\lambda_m)} \tag{44c}$$

4.2 A Seabed of Finite Thickness

Following the framework proposed by Jeng (1997) for regular waves and for the present two-dimensional problem, the random wave-induced pore pressure and displacements for finite soil thickness can be written as

$$p=\mathbf{Re}\left\{\sum_{m=1}^{M}\frac{p_b^{(m)}}{1-2\mu}\left[(1-\lambda_m-2\mu)\left(C_2^m e^{k_m z}-C_4^m e^{-k_m z}\right)\right.\right.$$
$$\left.\left.+(1-\mu)\left(\delta_m^2-k_m^2\right)\left(C_5^m e^{\delta_m z}+C_6^m e^{-\delta_m z}\right)\right]e^{i(k_m x-\omega_m t+\varepsilon_m)}\right\} \tag{45}$$

$$u=\mathbf{Re}\left\{\sum_{m=1}^{M}\frac{ip_b^{(m)}}{2Gk_m}\left[\left(C_1^m+C_2^m k_m z\right)e^{k_m z}+\left(C_3^m+C_4^m k_m z\right)e^{-k_m z}\right.\right.$$
$$\left.\left.+\left(C_5^m e^{\delta_m z}+C_6^m e^{-\delta_m z}\right)\right]e^{i(k_m x-\omega_m t+\varepsilon_m)}\right\} \tag{46}$$

$$w=\mathbf{Re}\left\{\sum_{m=1}^{M}\frac{p_b^{(m)}}{2Gk_m}\left\{\left[C_1^m-(1+2\lambda_m-k_m z)C_2^m\right]e^{k_m z}\right.\right.$$
$$-\left[C_3^m+(1+2\lambda_m+k_m z)C_4^m\right]e^{-k_m z}$$
$$\left.\left.+k_m\delta_m\left(C_5^m e^{\delta_m z}-C_6^m e^{-\delta_m z}\right)\right\}e^{i(k_m x-\omega_m t+\varepsilon_m)}\right\} \tag{47}$$

Coefficients δ_m and λ_m are expressed as Eq. (40).

Substituting Eqs. (46-47) into Eq. (30), the effective normal stresses σ_x', σ_z' and shear stress τ_{xz} can be determined as

$$\sigma_x'=\mathbf{Re}\left\{-\sum_{m=1}^{M}p_b^{(m)}\left[\left(C_1^m+C_2^m k_m z+\frac{2\mu\lambda_m}{1-2\mu}C_2^m\right)e^{k_m z}\right.\right.$$
$$+\left(C_3^m+C_4^m k_m z-\frac{2\mu\lambda_m}{1-2\mu}C_4^m\right)e^{-k_m z}$$
$$\left.\left.+\left(k_m^2-\frac{\mu(\delta_m^2-k_m^2)}{1-2\mu}\right)\left(C_5^m e^{\delta_m z}+C_6^m e^{-\delta_m z}\right)\right]e^{i(k_m x-\omega_m t+\varepsilon_m)}\right\} \tag{48}$$

$$\sigma_z'=\mathbf{Re}\left\{\sum_{m=1}^{M}p_b^{(m)}\left[\left(C_1^m+C_2^m k_m z-\frac{2\lambda_m(1-\mu)}{1-2\mu}C_2^m\right)e^{k_m z}\right.\right.$$
$$\left.\left.+\left(C_3^m+C_4^m k_m z-\frac{2\lambda_m(1-\mu)}{1-2\mu}C_4^m\right)e^{-k_m z}\right.\right.$$

$$+\frac{1}{1-2\mu}\left[\delta_m^2(1-\mu)-k_m^2\mu\right]\left(C_5^m e^{\delta_m z}+C_6^m e^{-\delta_m z}\right)\Bigg] e^{i(k_m x-\omega_m t+\varepsilon_m)} \Bigg\} \tag{49}$$

$$\tau_{xz}=\mathbf{Re}\Bigg\{ \sum_{m=1}^{M} ip_b^{(m)} \Big\{\left[C_1^m+(k_m z-\lambda_m)C_2^m\right]e^{k_m z}$$

$$-\left[C_3^m+(k_m z+\lambda_m)C_4^m\right]e^{-k_m z}$$

$$+k_m\delta_m\left(C_5^m e^{\delta_m z}-C_6^m e^{-\delta_m z}\right)\Big\} e^{i(k_m x-\omega_m t+\varepsilon_m)} \Bigg\} \tag{50}$$

In the expressions of (45)-(50), there are six resulting coefficients, C_1^m to C_6^m for each *m*-th component regular wave, whose values are systematically presented in Jeng (1997) for hydraulically anisotropic and unsaturated soil conditions.

5 RESULTS AND DISCUSSIONS

Based on the research methodology presented in Section 2 for random waves and Section 3 for soil response boundary value problem, the semi-analytical solutions for random wave-induced soil response of an infinite or finite soil thickness are presented in Section 4. Based on the general solutions, it is possible to investigate the effect of wave randomness on the wave-induced soil response. All the physical variables to be presented are non-dimensionalized with respect to the hydrostatic water pressure at the seabed $\gamma_w d$. The present numerical simulation is performed for a hydraulically isotropic coarse sand. Input data of the numerical examples are tabulated in Table 2, which includes significant wave height $H_{1/3}$, significant wave period $T_{1/3}$, water depth d, finite soil depth h, permeability K_x, K_z, soil porosity n', Poisson's ratio μ, shear modulus G, degree of saturation S_r and unit weight of submerged soil γ_s. All the calculations are based on these parameters unless specified otherwise.

Table 2 Input data of calculations

Wave characteristics			Soil characteristics						
$H_{1/3}$ (m)	$T_{1/3}$ (s)	d (m)	h (m)	$K_x = K_z$ (m/s)	n' (-)	μ (-)	G (N/m^2)	S_r (-)	γ_s (-)
6	10	25	12.5	0.01	0.3	1/3	10^7	0.975	2.0

5.1 Comparison between Regular and Random Wave-induced Soil Responses

By using the semi-analytical solutions in Section 4 and representative regular wave in Section 2.6 together with the parameters specified in the previous context, the comparison between regular and random wave-induced soil responses can be conducted for both infinite and finite soil thickness.

Figures 6 and 7 illustrate the time-varying normalized pore pressure p, effective normal stresses σ'_x, σ'_z and shear stress τ_{xz} variations in one random record for an

infinite soil thickness by using B-M spectrum at two different elevations, say, $z=-0.25L_r$ and $z=-0.5L_r$, respectively. Figures 8 and 9 are the corresponding results using JONSWAP spectrum. In these figures, two horizontal dashed lines represent the corresponding soil responses range under the representative regular wave loading. No doubt, for random wave loading, at some certain duration, i.e., $t=150$ s for B-M spectrum or $t=250$ s for JONSWAP spectrum, the wave-induced soil response is greater than the results of the regular waves at the same time due to wave irregularity owing to the wave randomness.

Taking into account the regular wave results, the relative soil response under random waves increases with the increase of soil depth. For example, various random wave-induced soil responses are just beyond the dashed-line limitation at $z=-0.25L_r$ shown in Fig. 6; however, such responses are much larger than the regular wave amplitude at $z=-0.5L_r$ shown in Fig. 7. At lower depth, soil responses are easier to overpass the dashed-line boundary of regular waves. Comparing with the regular wave cases, for random waves, soil response in the lower layers seems to be more active or has high possibility to be beyond the regular wave limitation. Similar scenario can also be observed in Figs. 8 and 9 for JONSWAP spectrum results.

From these figures, another interesting phenomenon can also be observed that with the increase of soil depth, the soil response becomes smooth. That means the high frequency part with small frequency spectra are suppressed with the increase of soil depth and can not be transmitted into the deep soil. For example, in Figs. 6 and 7 for pore pressure variation, around time $t=125$ s, the distribution of pressure becomes more harmonic and the small variation humps vanish with the increase of soil depth.

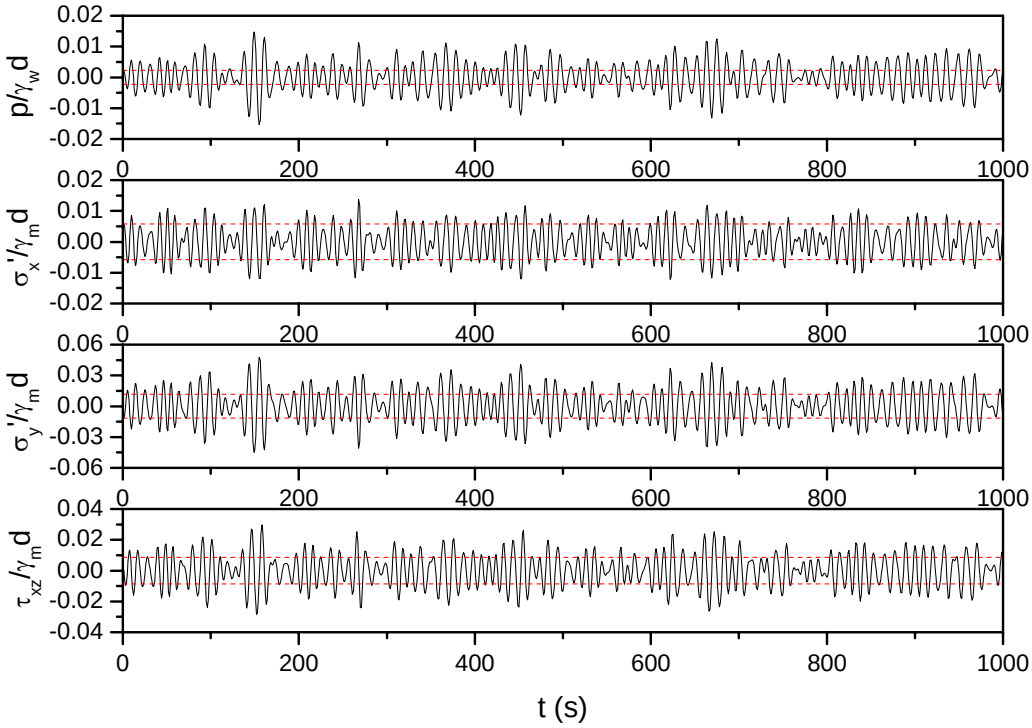

Fig. 6 Time-varying normalized pressure, effective normal stress and shear stress variations at level $z = -0.25L_r$ for infinite soil thickness using B-M spectrum.

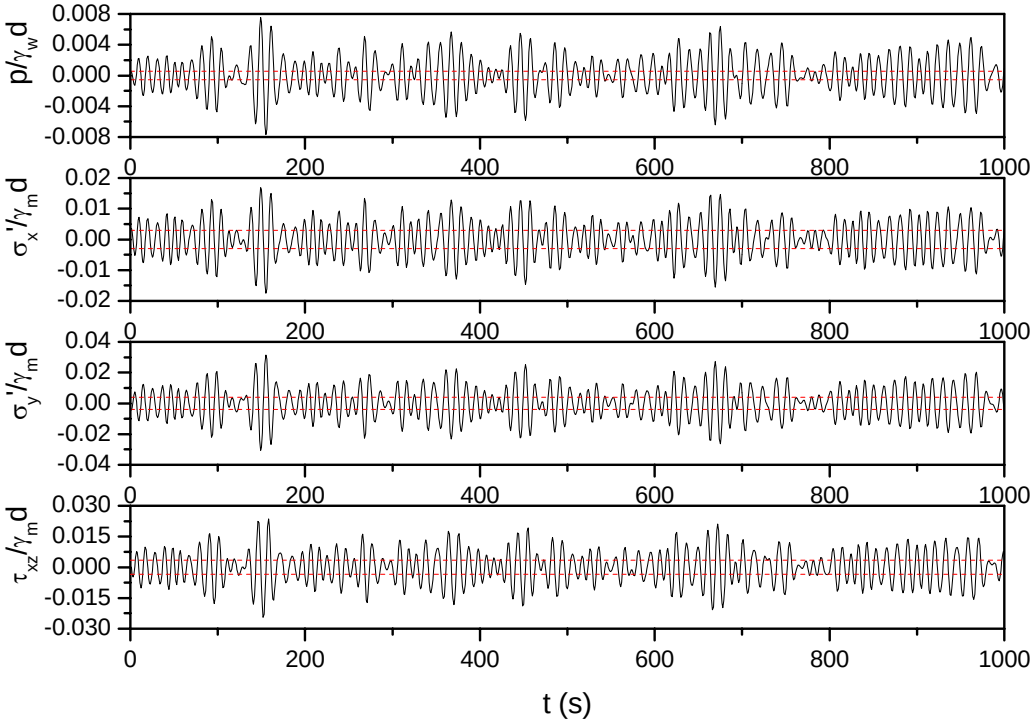

Fig. 7 Time-varying normalized pressure, effective normal stress and shear stress variations at level $z = -0.5L_r$ for infinite soil thickness using B-M spectrum.

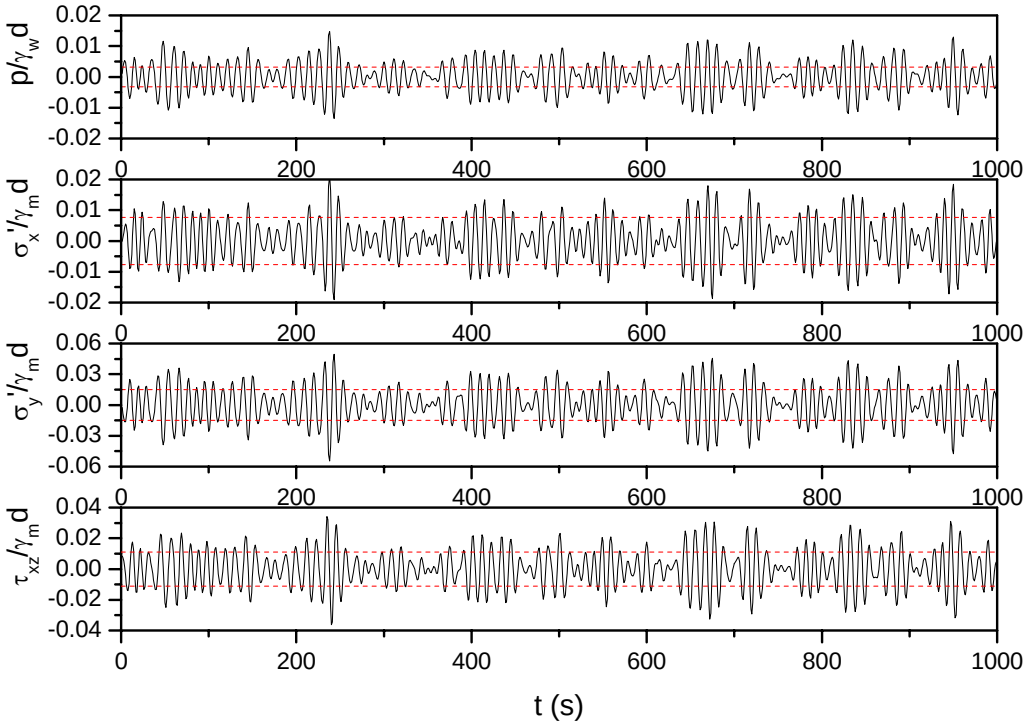

Fig. 8 Time-varying normalized pressure, effective normal stress and shear stress variations at level $z = -0.25L_r$ for infinite soil thickness using JONSWAP spectrum.

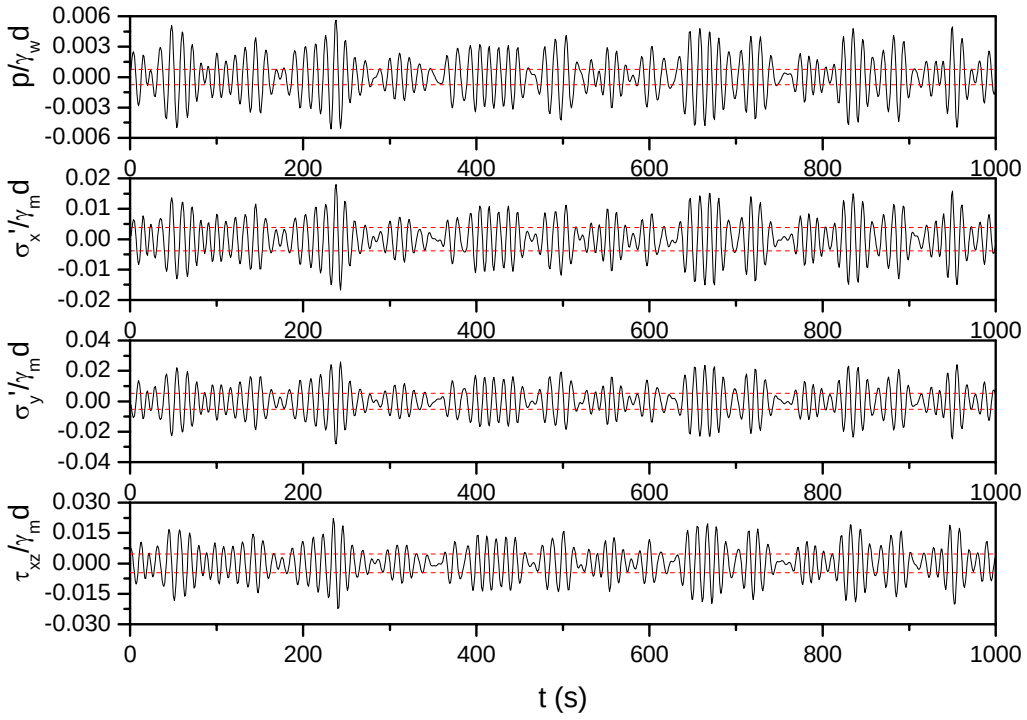

Fig. 9 Time-varying normalized pressure, effective normal stress and shear stress variations at level $z = -0.5L_r$ for infinite soil thickness using JONSWAP spectrum.

Figure 10 demonstrates the time-varying normalized pore pressure $p/\gamma_w d$ distribution of a finite soil thickness within one wave record by using B-M spectrum. The upper panel illustrates the results at $z=-0.5h$, while the lower panel is for the soil response at the rigid impermeable bottom, i.e., $z=-h$. In the figure, two horizontal dashed lines represent the soil response range under the representative regular wave loading at the relevant elevations. The corresponding results using JONSWAP spectrum is shown in Figure 11. From these two figures, the irregularity of pore pressure variation caused by the wave randomness can be clearly observed. For random wave loading, at some specified time, the wave induced pore pressure is greater than the results of regular waves at the same time. Comparing the results at $z=-0.5h$ and $z=-h$, we see that the pore pressure values are decreasing with the increase of soil depth $|z/h|$, which shows that the spatial distribution of the random wave-induced pore pressure occurs in much the same way as in the case of regular waves since the dashed line range also becomes smaller as $|z/h|$ increases.

Considering the difference between B-M and JONSWAP spectra results in Figures 10 and 11, we can see the irregularity of the temporal pore pressure variation is more significant for JONSWAP spectrum case, which can be confirmed through the standard deviation of the simulated results. The mean values of the pore pressure variation at different depths are almost zero. For B-M spectrum, the standard deviation of normalized pore pressure distribution at $z=-0.5h$ is 0.016, and 0.012 at $z=-h$. Both are smaller than the corresponding values for JONSWAP spectrum, which are 0.018 and 0.013 respectively. The temporal pore pressure variation under the JONSWAP spectrum is more active with large fluctuations along the time history.

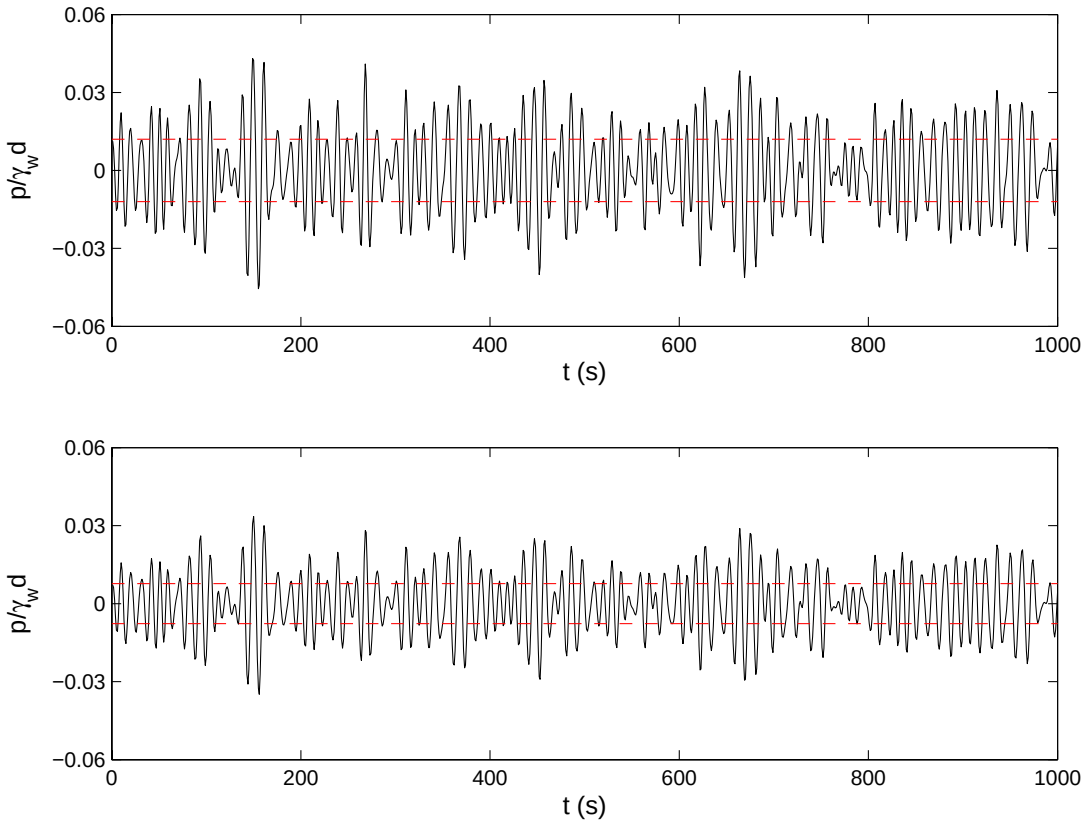

Fig. 10 Time-varying normalized pore pressure distribution of a finite soil thickness using B-M spectrum: $z = -0.5h$ (upper panel) and $z = -h$ (lower panel).

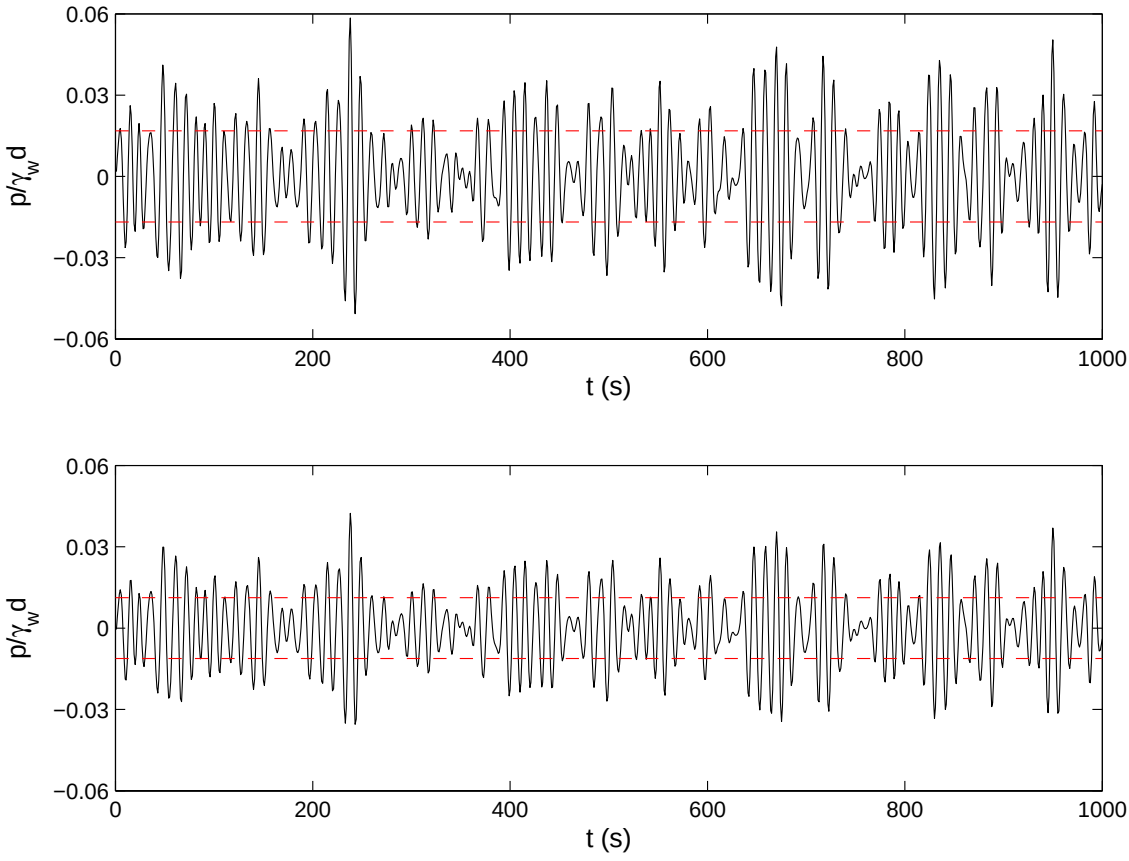

Fig. 11 Time-varying normalized pore pressure distribution of a finite soil thickness using JONSWAP spectrum: $z = -0.5h$ (upper panel) and $z = -h$ (lower panel).

For the engineering practice, it is important to investigate the vertical distribution of the maximum soil responses. Figure 12 presents such results under the random and representative regular wave loadings, which include the pore pressure, the horizontal and vertical effective normal stresses and shear stress. Due to the wave randomness, the maximum random wave-induced soil response is larger than the corresponding representative regular wave results. However, the vertical distribution tendency is the same for these two wave loadings. i.e., maximum pore pressure $p_m/\gamma_w d$ is attenuating with the increase of soil depth $|z/h|$. Looking at the results of representative regular waves, we can see that the soil responses for the "JONSWAP" regular wave (JRW) are larger than that of "B-M" regular wave (BRW). This is because that the longer JRW period as mentioned in Section 2.6, which induced a smaller wave number due to longer wavelength. Hence, the amplitude of pore pressure at the seabed is larger for JRW case.

Further investigating the results of random waves, in general, the maximum soil responses under the JONSWAP spectrum are still greater than the B-M spectrum cases although the significant wave height and period are the same for these two different spectra. Taking figure 5 into account, the maximum frequency spectra $S(f)$, which is related to the maximum component wave energy or wave height, is much larger for JONSWAP spectrum than for B-M spectrum. Considering the significant wave period, which is almost equal to the maximum component wave period (Goda, 2000), is same for these two spectra, the maximum pore pressure at the seabed is larger for JONSWAP spectrum due to aforementioned larger wave height. This means under the same wave and soil characteristics, the JONSWAP type random waves introduce more significant soil responses within the marine sediments.

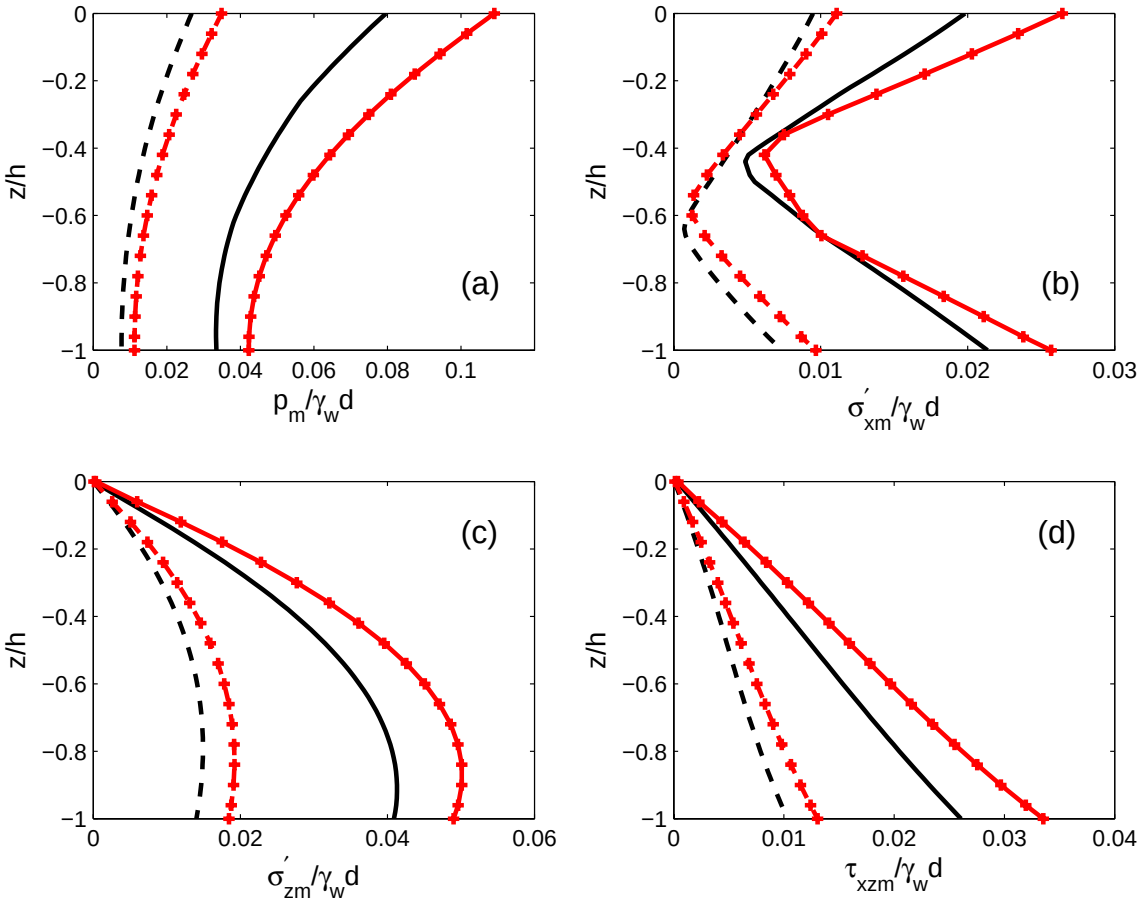

Fig. 12 Vertical distribution of the maximum soil responses under the random waves ('–+–' for JONSWAP spectrum and '—' for B-M spectrum) and representative regular wave ('– + –' for JONSWAP spectrum and '- -' for B-M spectrum) loadings. (a) pore pressure p_m (b) horizontal effective normal stress σ'_{xm} (c) vertical effective normal stress σ'_{zm} (d) shear stress τ_{xzm}.

Figure 13 illustrates vertical distribution of relative maximum soil responses between random and representative regular wave loadings ($\Delta x_m = x_{mi} - x_{mr}$, where x_{mi} and x_{mr} denote the irregular/random and regular wave-induced soil response respectively) in case of B-M and JONSWAP spectra. Considering the present finite soil depth with $d = 0.5h$, for pore pressure, the difference between random and regular wave results is decreasing with increase of $|z/h|$, while for shear stress, it is increasing with $|z/h|$ in the present simulated soil depth. Considering the results between B-M and JONSWAP spectra, the pore pressure difference is decreasing as $|z/h|$ increases;

the shear stress difference is increasing with $|z/h|$. However, with the increase of soil depth, the relative soil response difference (between the random and regular waves or different type random waves) will decrease because various soil responses go to zero at the infinite depth, which will be further discussed in the following section.

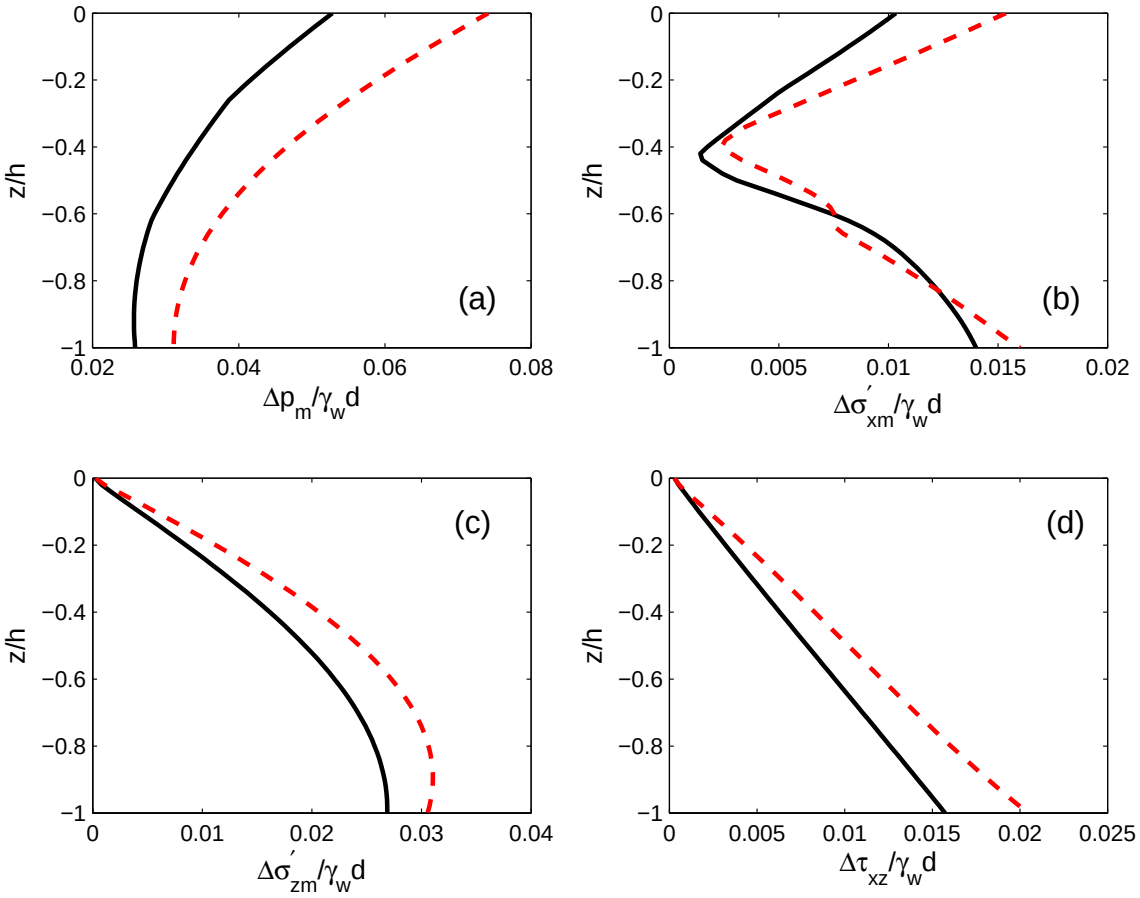

Fig. 13 Vertical distribution of relative maximum soil responses between random and representative regular wave loadings (solid lines for B-M spectrum and dashed lines for JONSWAP spectrum). (a) relative pore pressure Δp_m (b) relative horizontal effective normal stress $\Delta\sigma'_{xm}$ (c) relative vertical effective normal stress $\Delta\sigma'_{zm}$ (d) relative shear stress $\Delta\tau_{xzm}$.

5.2 Effect of Soil Parameters on Random Wave-induced Soil Response

In this section, the influence of two key soil parameters, i.e., the degree of saturation S_r and vertical soil permeability K_z, on the random wave-induced soil response will

be investigated. The numerical calculation is performed under the same wave and soil characteristics listed in the previous section unless specified otherwise. For simplicity, the discussion is only for the random wave results under the B-M frequency spectrum.

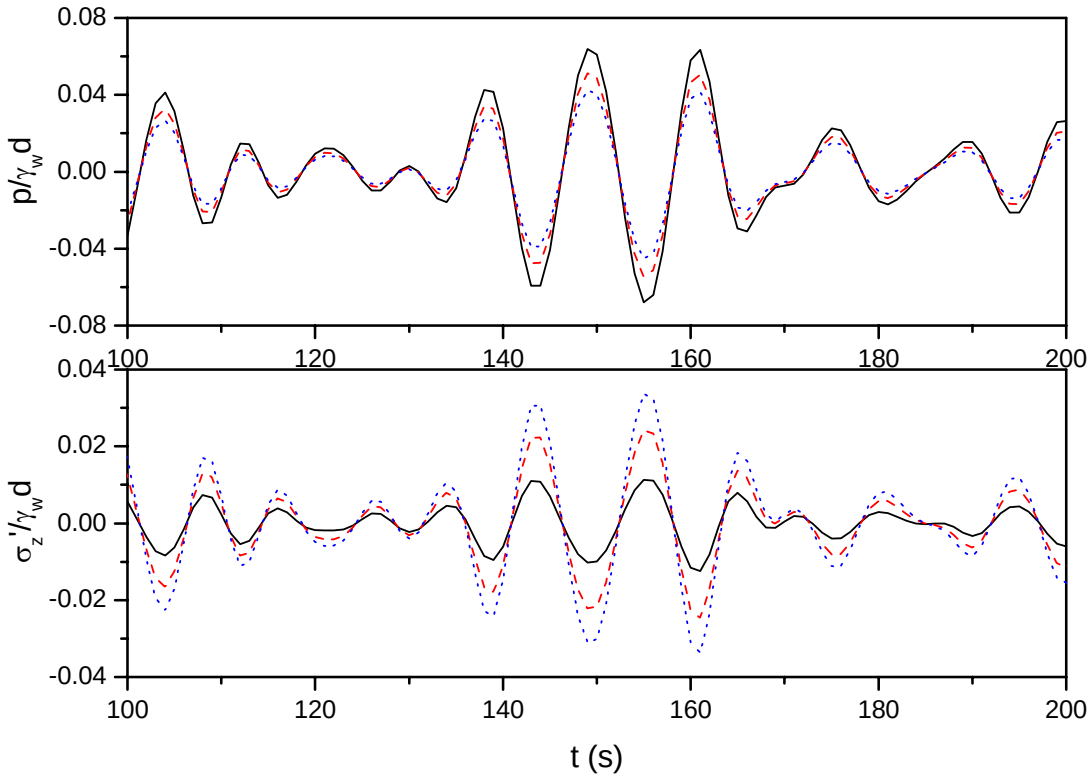

Fig. 14 Time-varying normalized pore pressure (upper panel) and effective vertical normal stress (lower panel) distributions for three different degrees of soil saturation. '—' for $S_r = 1.0$; '- -' for $S_r = 0.975$; '···' for $S_r = 0.95$ (infinite thickness).

For Figs. 14 and 15, the numerical calculation is performed for an infinite soil thickness at the level $z / L_r = 0.05$, above which is the region likely to be liquefied (Hsu, et al., 1993). Figure 14 illustrates the time-varying normalized pore pressure p and effective vertical normal stress σ_z' distributions for three different soil saturations, i.e., $S_r = 1.0$, $S_r = 0.975$ and $S_r = 0.95$. General speaking, the wave-induced pore pressure decreases as the degree of saturation decreases, while an opposite trend is observed for the vertical effective normal stress.

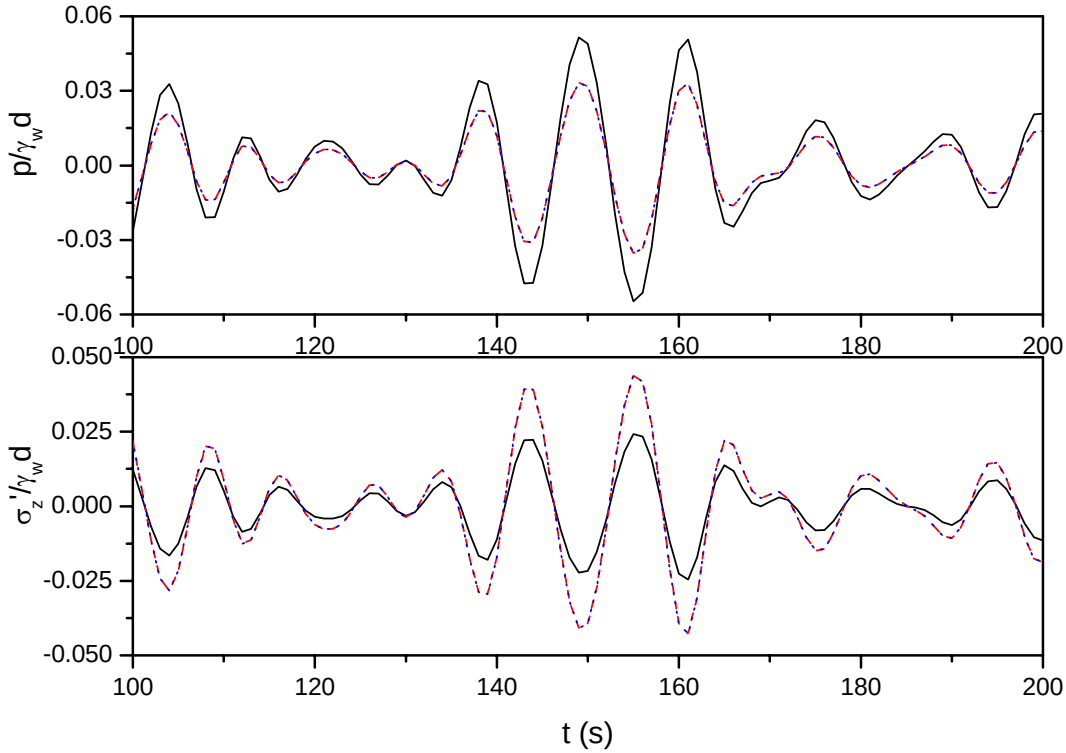

Fig. 15 Time-varying normalized pore pressure (upper panel) and effective vertical normal stress (lower panel) distributions for three different vertical soil permeabilities. '—' for $K_z = 10^{-2}$ m/s; '- -' for $K_z = 10^{-4}$ m/s; '...' for $K_z = 10^{-6}$ m/s (infinite thickness).

Soil permeability is another important parameters, which directly affect the wave-induced soil response. Figure 15 presents the distribution of the pore pressure and vertical effective normal stress for three different soil permeabilities, i.e., $K_z = 10^{-2}$ m/s, $K_z = 10^{-4}$ m/s and $K_z = 10^{-6}$ m/s. As shown in the figure, there is a significant difference between the results of $K_z = 10^{-2}$ m/s and $K_z = 10^{-4}$ m/s with pore pressure being larger and vertical effective stress being smaller for higher soil permeability, while the difference between $K_z = 10^{-4}$ m/s and $K_z = 10^{-6}$ m/s is ambiguous.

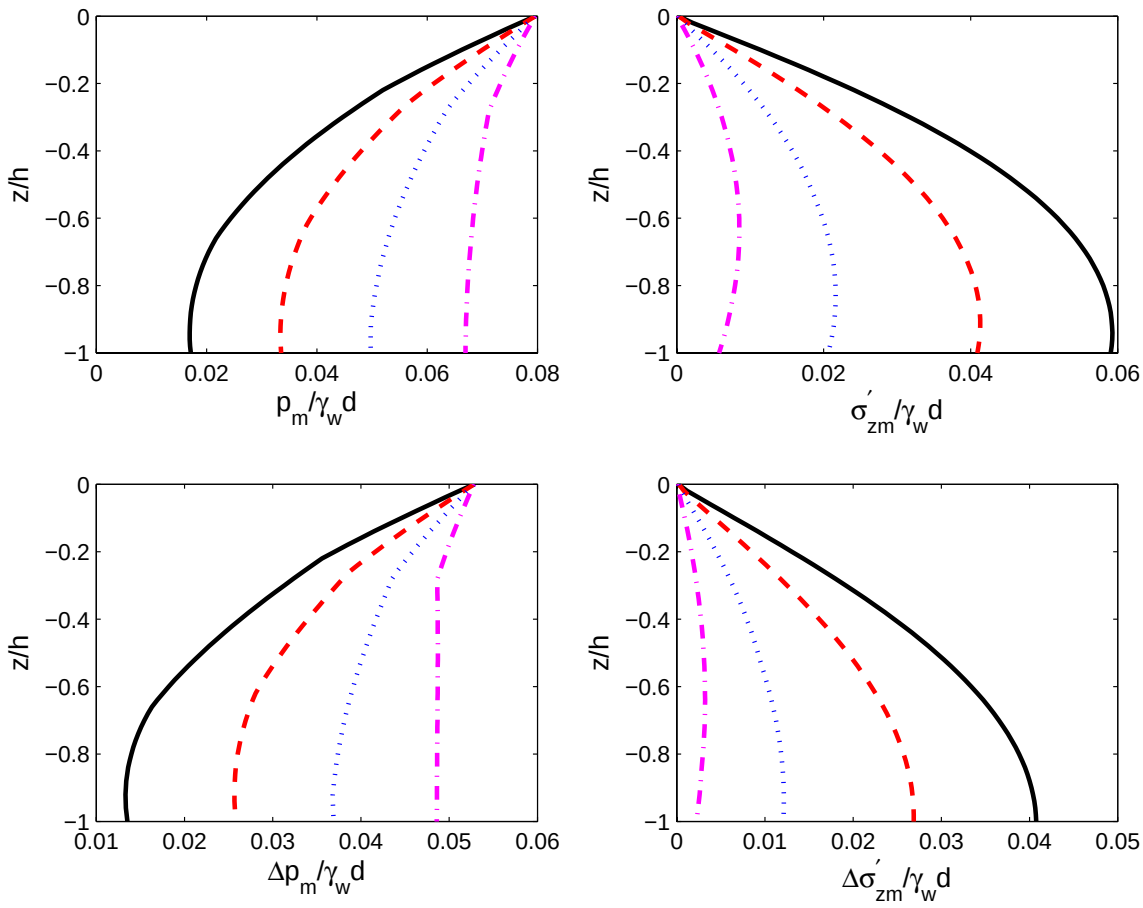

Fig. 16 Vertical distribution of p_m (left panels) and σ'_{zm} (right panels) for random wave results (upper panels) and relative results (lower panels) under different degrees of saturation. Solid lines for $S_r = 0.95$, dashed lines for $S_r = 0.975$, dotted lines for $S_r = 0.99$ and dashed-dotted lines for $S_r = 1.0$. (finite thickness).

For Figs. 16 and 17, the numerical calculation is performed for a finite soil thickness. As mentioned previously, it is important to investigate the vertical profile of the maximum soil response. In the following analysis, we will only focus on two kinds of soil responses, maximum pore pressure p_m and maximum vertical effective normal stress σ'_{zm}.

Figure 16 demonstrates the effect of degree of saturation on the maximum random wave-induced soil response as well as the relative difference between random and regular waves. Four degrees of saturation are considered here, e.g., $S_r = 0.95$, 0.975, 0.99 and 1.0. With the increase of the degree of saturation, p_m increases and

σ'_{zm} decreases along the vertical depth. Considering the relative difference between random and regular wave loadings, same conclusions can be obtained because the regular wave-induced soil responses present the same tendency with rather small values.

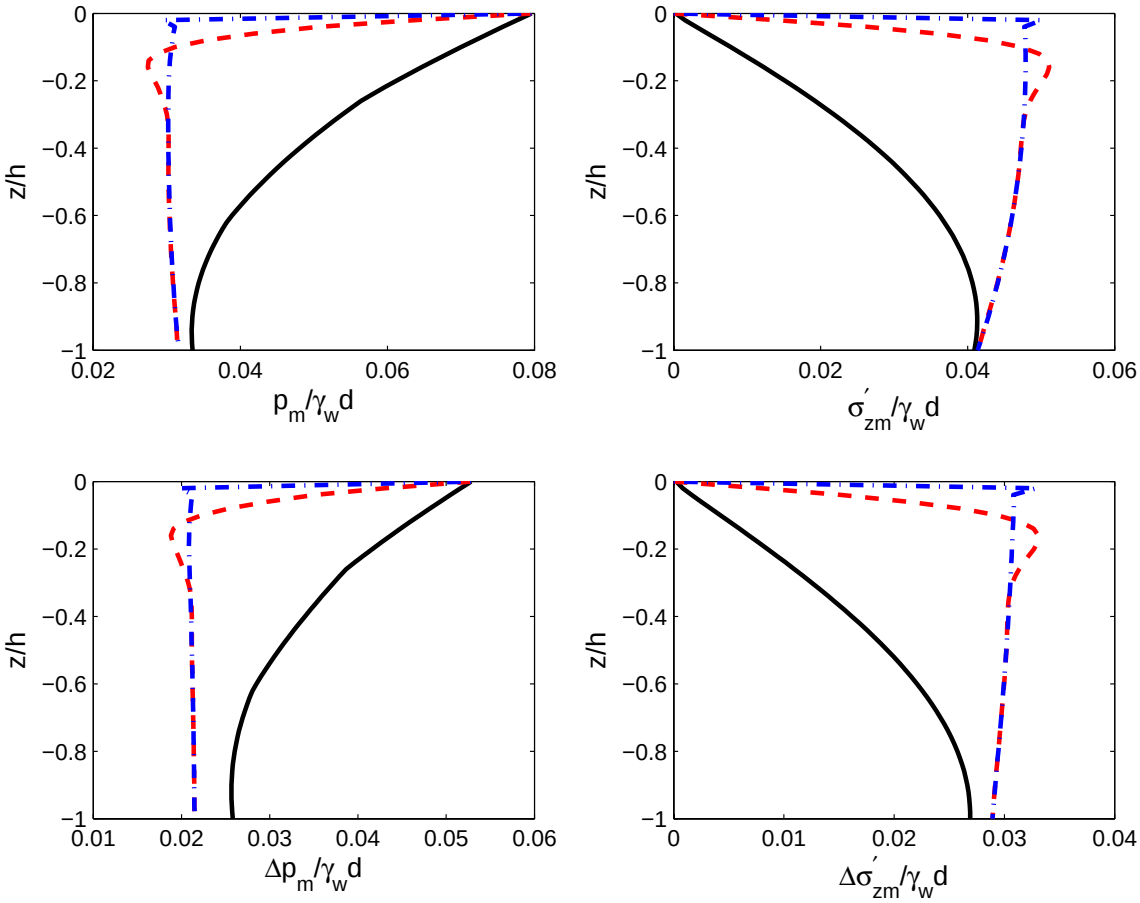

Fig. 17 Vertical distribution of p_m (left panels) and σ'_{zm} (right panels) for random wave results (upper panels) and relative results (lower panels) under different soil permeabilities. Solid lines for $K_z = 10^{-2}$ m/s, dashed lines for $K_z = 10^{-4}$ m/s and dashed-dotted lines for $K_z = 10^{-6}$ m/s. (finite thickness).

Figure 17 presents the influence of soil permeability on the maximum random wave-induced soil responses together with the relative difference between random and regular wave-induced results. Three different soil permeabilities are utilized, i.e., $K_z = 10^{-2}$ m/s for coarse sand, $K_z = 10^{-4}$ m/s for fine sand and $K_z = 10^{-6}$ m/s for silt. With the decrease of soil permeability, p_m decreases and σ'_{zm} increases. The

difference between fine sand and silt is negligible except at the vicinity of seabed where there is a sudden decrease for p_m and increase for σ'_{zm}. For coarse sand, the spatial distribution of soil response is more gentle. Similar results occur for Δp_m and $\Delta\sigma'_{zm}$, which indicate the random wave-induced soil response is in the much same way as the regular wave cases.

5.3 Effect of Wave Characteristics on Random Wave-induced Soil Response

In this section, the influence of two random wave parameters, i.e., significant wave height $H_{1/3}$ and wave period $T_{1/3}$, on the random wave-induced soil response of a finite soil thickness will be investigated.

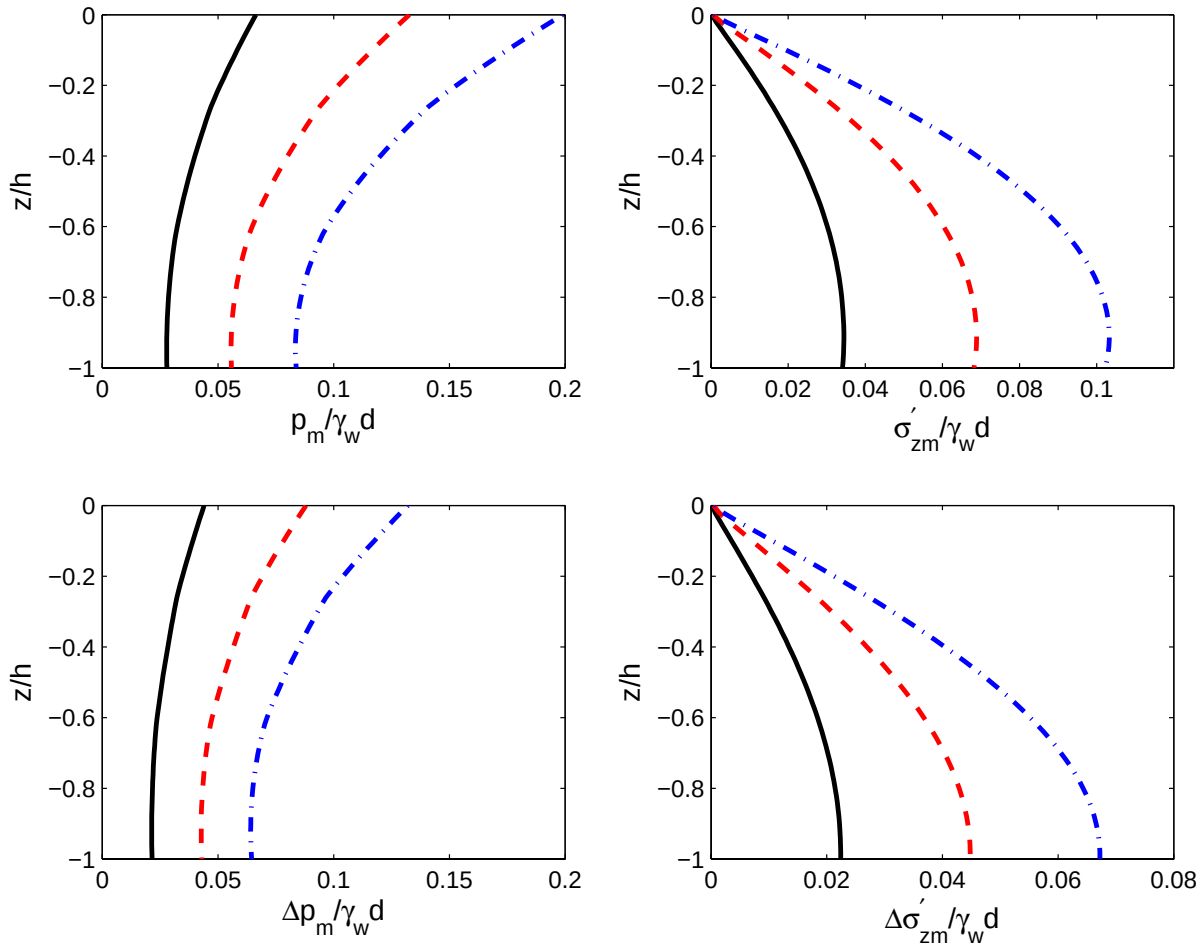

Fig. 18 Vertical distribution of p_m (left panels) and σ'_{zm} (right panels) for random wave results (upper panels) and relative results (lower panels) under different significant wave heights. Solid lines for $H_{1/3}=5$ m, dashed lines for $H_{1/3}=10$ m and dashed-dotted lines for $H_{1/3}=15$ m. (finite thickness).

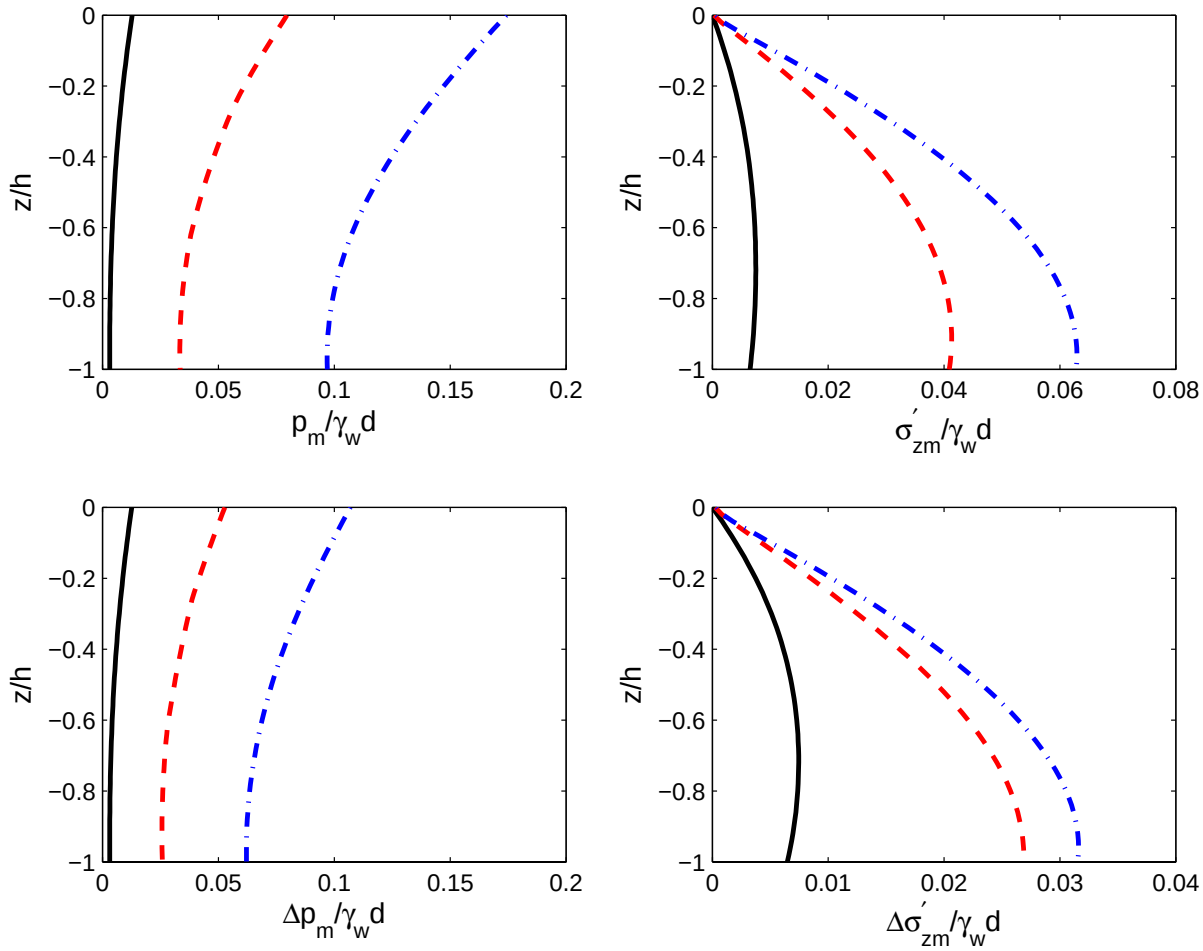

Fig. 19 Vertical distribution of p_m (left panels) and σ'_{zm} (right panels) for random wave results (upper panels) and relative results (lower panels) under different significant wave periods. Solid lines for $T_{1/3}=5$ s, dashed lines for $T_{1/3}=10$ s and dashed-dotted lines for $T_{1/3}=20$ s. (finite thickness).

Figure 18 shows the influence of significant wave height on maximum random wave-induced soil response. Three typical wave heights (before wave breaking) are utilized here, i.e., $H_{1/3}=0.2d$, $0.4d$ and $0.6d$. Figure 19 presents the influence of significant wave period. Three wave periods are applied, i.e., $T_s=5$s, $T_s=10$ s and $T_s=20$ s. From these two figures, we can see: with the increase of $H_{1/3}$ and $T_{1/3}$, both p_m and σ'_{zm} increase due to the increase of pore pressure at the seabed. Looking at the relative difference between the random and regular waves, similar scenario can be observed, which further proves that the effect of wave

characteristics on the maximum random wave-induced soil response are similar to the regular wave cases.

5.4 Effect of Soil Thickness on Random Wave-induced Soil Response

The influence of soil thickness on the random wave-induced maximum soil responses is investigated and illustrated in Figure 20. Different finite soil thicknesses together with the results under infinite soil depth (dashed lines) are presented in the figure.

In the vicinity of seabed, the soil responses for different soil depths are almost uniform. Different seabed thicknesses affect the soil response around the rigid impermeable bottom. Comparing with the infinite soil depth results, for finite soil depth, the maximum pore pressure around the rigid bottom increases. With the increase of soil depth, the vertical pore pressure distribution is approaching the results under the infinite soil depth. As for vertical effective normal stress σ'_{zm}, with the increase of soil thickness, its value first increases from the case $h/d = 0.25$ to $h/d = 2.0$; while σ'_{zm} decreases somewhat from $h/d = 2.0$ to $h/d = 4.0$. Further increase the soil thickness, the σ'_{zm} value decreases and its profile approaches the results for infinite soil depth. For small seabed thickness ($h/d = 0.25$ and 0.5), the σ'_{zm} profile still cannot completely developed before reaching the rigid bottom. After the σ'_{zm} profile entirely grows ($h/d = 1.0$), the influence of rigid bottom becomes significant, which "compresses" the vertical σ'_{zm} distribution and makes the profile more forwardly protuberant. This makes the maximum value of σ'_{zm} for case $h/d = 2.0$ around level $z/d = 0.7$ larger than the infinite result. Further increase the soil thickness, such "compression" due to finite seabed thickness releases gradually, and soil can hardly "feel" the existence of rigid impermeable bottom. Hence, the maximum value of σ'_{zm} decreases, and finally σ'_{zm} profile returns back to the infinite case.

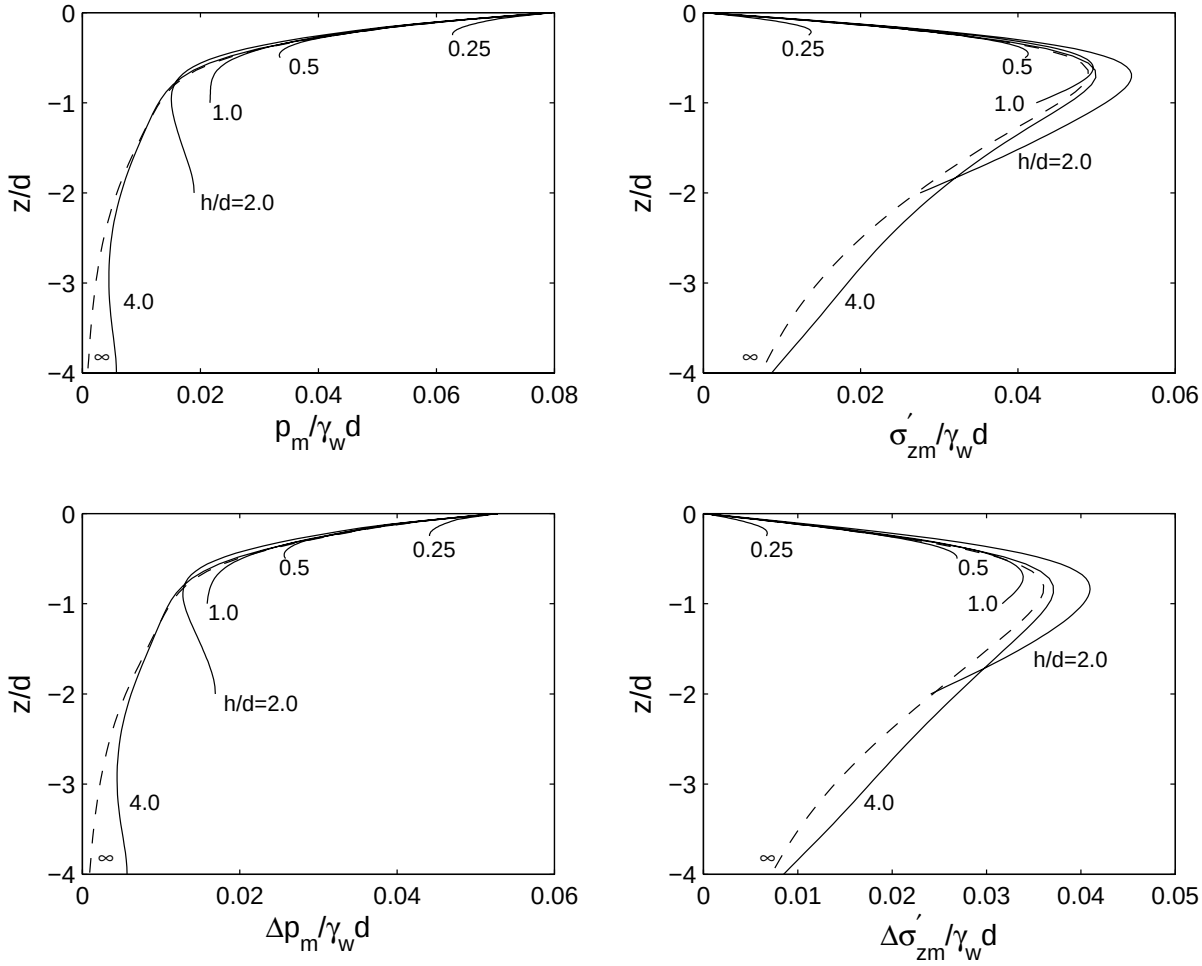

Fig. 20 Vertical distribution of p_m (left panels) and σ'_{zm} (right panels) for random wave results (upper panels) and relative results (lower panels) under different soil thickness. Dashed lines represent the results under the infinite soil thickness.

5.5 Random Wave-induced Liquefaction

It has been conceived that the soil will be liquefied when the vertical effective stress vanishes, thus losing its strength to carry any load, and consequently causing seabed instability. Such liquefaction generally occurs at the time when wave trough is passing by (Jeng, 1997). There exist various criteria to judge the liquefied state in a porous seabed. After inter-comparison with the previous field experimental measurements, Jeng (1997) suggested the following criterion

$$-\frac{1}{3}(\gamma_s-\gamma_w)(1+2K_0)z+(p_b-p(z))\le 0 \tag{51}$$

where γ_s is the unit weight of soil, K_0 is the coefficient of earth pressure at rest and is related to the Poisson's ratio μ as (Okusa, 1985)

$$K_0 = \frac{\mu}{1-\mu} \tag{52}$$

where p_b and $p(z)$ represent the pore pressure at the seabed and certain depth z, whose expressions are presented in Eqs. (36) and (37) for an infinite soil thickness or (45) for a finite soil thickness respectively. In Eq. (51), the first term represents the average effective geostatic stress cause by the self weight of the soil, while the second term denotes the excess pore pressure induced by the random wave system on the seafloor.

Considering the engineering practice, it is more interesting to examine the maximum liquefaction depth Z_L, which is important for many coastal engineering installations. To investigate the random wave-induced maximum liquefaction depth, we use the same wave and soil parameters specified previously except the soil permeability K_x, K_z and the degree of saturation S_r. Jeng (1997) found a seabed with lower permeability is more easily liquefied than a seabed with higher permeability. From his calculation, no liquefaction occurs in a seabed with permeability larger than 10^{-3} m/s. Here, we propose an isotropic fine sand with permeability $K_x = K_z = 10^{-4}$ m/s in the present numerical calculation. The degree of saturation S_r varies from 0.95 to 1.0 to investigate the effect of S_r on liquefaction depth.

Figure 21 demonstrates the distribution of maximum liquefaction depth Z_L with the variation of the degree of saturation S_r for regular and random wave loadings. It is clear that for the same S_r, random wave-induced Z_L is much larger than the corresponding representative regular wave-induced Z_L due to the influence of wave randomness (around 2.5-3.0 times for the present simulation at $S_r = 0.95$). With the increase of S_r, Z_L decreases with a more rapid drop for large S_r values. Considering the representative regular waves, Z_L touches zero value earlier than the random wave cases. For example, considering B-M spectrum case, regular wave-induced Z_L becomes equal to zero after $S_r = 0.974$ where there still exists a

large Z_L value for random wave loading ($Z_L = 1.95$ m), which further demonstrates the significant enhancement on the liquefaction depth from random waves. Another point is that comparing with the regular wave results, same Z_L can occur for relative large degree of saturation under the random wave loading.

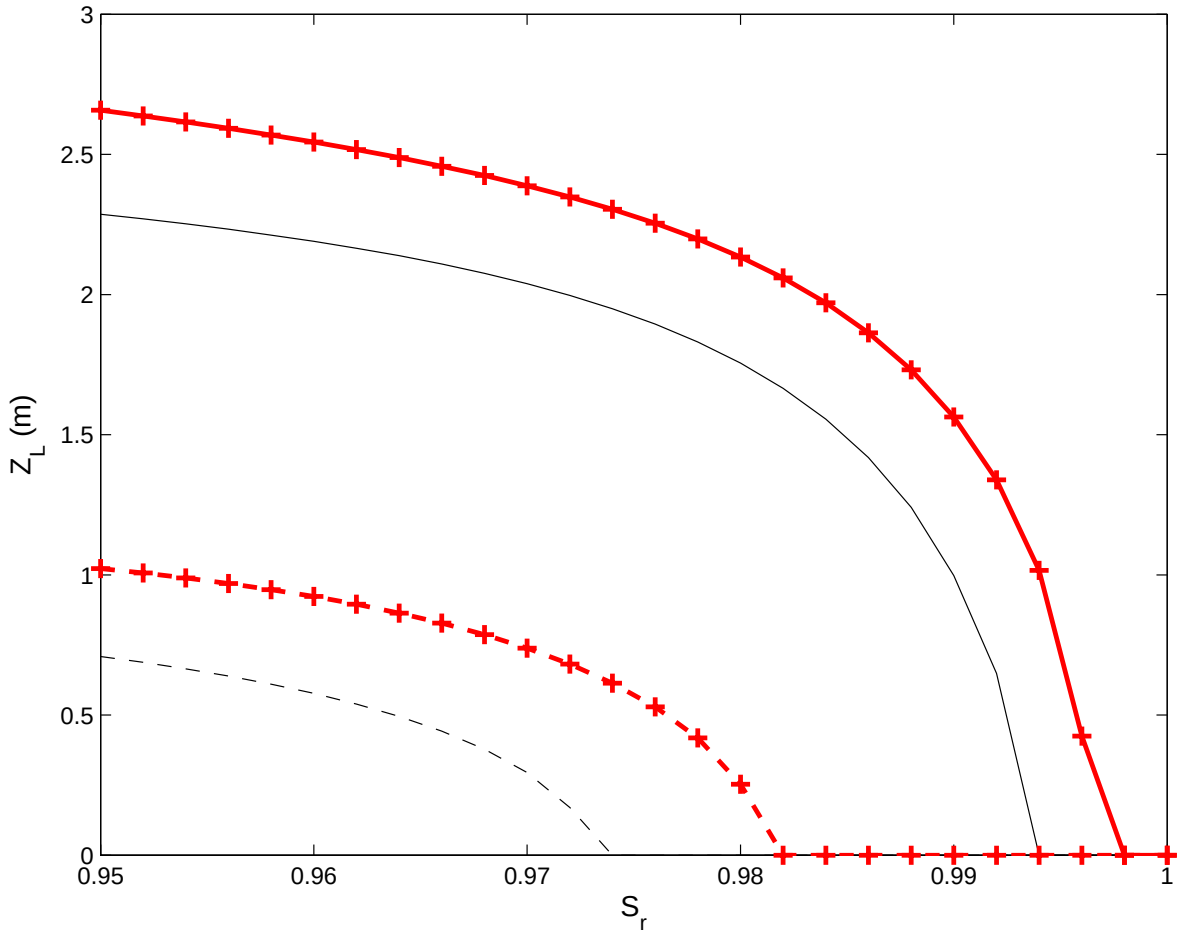

Fig. 21 Distribution of maximum liquefaction depth Z_L vs the degree of saturation S_r for regular and random wave loadings. Notation: random waves ('–+–' for JONSWAP spectrum and '—' for B-M spectrum); representative regular wave ('– + –' for JONSWAP spectrum and '- -' for B-M spectrum). (finite soil thickness).

As for the difference between the B-M and JONSWAP spectra (although the same significant wave height and period are applied), the explanation is similar to the different soil response results as specified in Figure 6. Considering the

representative regular wave (RRW) results, the RRW period is longer for JONSWAP spectrum, which induces larger pore pressure inside the seabed and causes deeper seabed liquefaction than the case for B-M spectrum RRW results under the same degree of saturation. Further focusing on the random wave results, Z_L under JONSWAP spectrum is larger than the B-M spectrum results. This is due to the large maximum frequency spectra $S(f)$ for JONSWAP spectrum, which introduces large pore pressure and higher liquefaction potential within marine sediments. Hence, considering the maximum liquefaction depth, we can see that comparing with the B-M type random waves, the JONSWAP type random wave loadings are more damaging under the same wave and soil conditions.

6 CONCLUSIONS

In this report, different from the conventional investigations on the soil responses under the linear regular wave loadings, various random wave-induced soil responses are examined. A simple analytical solution for the random wave-induced soil response (including the soil displacement, pore pressure, effective normal stresses and shear stress) is proposed for a two-dimensional hydraulically anisotropic and unsaturated soil condition with an infinite or finite seabed thickness. Two typical frequency spectra, B-M spectrum and JONSWAP spectrum, are adopted for random wave generation. Based on the calculation and discussion presented above, the main conclusions can be summarized as

(1) Time-varying random wave-induced soil response shows clear irregularity due to wave randomness. Such irregularity is more significant for random waves under JONSWAP frequency spectrum with large fluctuations along the time history. The temporal random wave-induced soil response frequently exceeds the results under the corresponding representative regular waves.

(2) Considering the vertical distribution of various maximum soil responses, random wave results present the similar tendency as the regular wave cases with a large maximum soil response magnitude due to wave randomness. Under the same wave and soil characteristics, the JONSWAP type random waves introduce more significant soil responses within the marine sediments than B-M type random waves.

(3) As for the effect of various soil and wave characteristics on the random wave-induced soil response, i.e., the degree of saturation, soil permeability, wave height and period, and considering the relative difference between random and relevant regular wave results, the present discussion indicates such parametric influence on the random wave-induced maximum soil response is in the much same way as that for the regular wave cases.

(4) The influence of soil thickness is also conducted, which demonstrates that due to the effect of rigid impermeable bottom, pore pressure increases around the bottom comparing with the infinite soil depth result at the same level. As for the maximum effective normal stress σ'_{zm} vertical distribution, for certain seabed thickness, i.e., $h/d = 2.0$, the σ'_{zm} distribution is compressed

by the rigid bottom, which yields a even larger maximum value of σ'_{zm} comparing to the infinite soil thickness result. However, further increasing the seabed thickness, all kinds of soil responses approach the results under the infinite soil depth.

(5) Finally, the random wave-induced maximum liquefaction depth Z_L is investigated and compared with the representative regular wave results. For the same degree of saturation, random wave-induced Z_L is much larger than the corresponding representative regular wave-induced Z_L . Otherwise, same Z_L can occur for a relative high degree of saturation under the random wave loadings. Comparing with the B-M type random waves, the JONSWAP type random waves are more damaging with a larger maximum liquefaction depth under the same wave and soil conditions.

REFERENCES

Boit, M.A., 1941. General theory of three-dimensional consolidation. Journal of Applied Physics, 12, 155-164.

Cheng, L., Sumer, B.M., Fredsøe, J., 2001. Solutions of pore pressure buildup due to progressive waves. International Journal of Numerical and Analytical Methods in Geomechanics, 25(9), 885-907.

Goda, Y., 2000. Random seas and design of marine structures. World Scientific Press, Singapore.

Hsu, J.R.C., Jeng, D.S., Tsai, C.P., 1993. Short-crested wave-induced soil response in a porous seabed of infinite thickness. Inter. J. of Numerical and Analytical Methods in Geomechanics, 17(8), 553-576.

Hsui, Y., Helfrich, S.C., 1983. Wave-induced pore pressures in submerged sand layer. Jorunal of Geotechnical Engineering, ASCE, 109(4), 603-618.

Jeng, D.S., Hsu, J.R.C., 1996. Wave-induced soil response in a nearly saturated sea-bed of finite thickness. Géotechnique, 46(3), 427-440.

Jeng, D.S., 1997. Wave-induced seabed response in front of a breakwater. PhD thesis, the University of Western Australia, pp297.

Longuet-Higgins, M.S., 1957. The statistical analysis of a random, moving surface. Philos. Trans. R. Soc. London, A, 249, 321-387.

Madsen, O.S., 1978. Wave-induced pore pressures and effective stresses in a porous bed. Géotechnique, 28(4), 377-393.

Mei, C.C., Foda, M.A., 1981. Wave-induced responses in a fluid-filled poro-elastic solid with a free surface – a boundary layer theory. Geophys, J. R. Astr. Soc., 66, 597-631.

Moshagen, H., Tørum, A., 1975. Wave induced pressures in permeable seabeds. Jorunal of the Waterways, Harbors and Coastal Engineering Division, ASCE, 101(WW1), 49-57.

Okusa, S. 1985. Wave-induced stresses in unsaturated submarine sediments. Géotechnique, 35, 517-532.

Oldham, C.E., Laery, P.S., 1999. Porewater nutrient fluxes in a shallow fetch-limited estuary. Marine Ecology Progress Series, 183(4), 39-47.

Sleath, J.F.A., 1970. Wave-induced pressures in beds of sand. Journal of Hydraulics Division, ASCE, 96(HY2), 367-378.

Sumer, B.M., Fredsøe, J., Christensen, S., Lind, M.T., 1999. Sinking/floatation of pipelines and other objects in liquefied soil under waves. Coastal Engineering, 38, 53-90.

Sumer, B.M., Fredsøe, J., 2002. The mechanics of scour in the marine environment. World Scientific Press, Singapore.

Thomas, C.P., 1995. A finite element model for the analysis of wave induced stresses, displacements and pore pressures in an unsaturated seabed II: model verification. Computers and Geotechnics, 17, 107-132.

Wang, Z. Luan, M., Liu, Z., Wang, D., 2005. Numerical analysis of dynamic response of seabed under random wave loading. Frontiers in offshore Geotechnics: ISFOG 2005, Taylor & Francis, London, 589-594.

Yamamoto, T., Koning, H.L., Sellmeijer, H., Van Hijum, E., 1978. On the response of a poro-elastic bed to water waves. J. Fluid Mechanics, 87, 193-206.

Yu, Y., 1992. Random waves and engineering application. Dalian Univ. of Technology Press, China. (in Chinese)

Zienkiewicz, O.C., Chang, C.T., 1980. Drained, undrained, consolidating and dynamic behavior assumptions in soils. Géotechnique, 30(4), 385-395.

APPENDIX I: User Manual of the Fortran Program Code

A.1 Main Program:

File "RAN_LIQ.IN" is the input file in which the physical meanings of various parameters have been specified in the file.

1. Parameter 'N' is for the total number of waves in the linear superposition, i.e., M in Eq. (1)
2. Parameter 'NN' is for time length of the simulated random wave record (Δt is assumed to be 1 s in the program)
3. Parameter 'GAMA' is for peak enhancement factor of JONSWAP spectrum, i.e., γ in Eq. (6d)
4. Array 'AMP' is for the wave amplitude of every sinusoidal wave component, i.e., a_i in Eq. (1)
5. Array 'EPS' is for the initial phase angle of every sinusoidal wave component, i.e., ε_i in Eq. (1)
6. Array 'PER' is for the wave period of every sinusoidal wave component.
7. Array 'TT' is for the time of the simulated random wave record

A.2 Subroutine 'WSPECTR'

1. Parameter 'M' is for wave validation, i.e., m in Eq. (10)
2. Array 'SUR' is for random wave surface elevation
3. Array 'SPS' is for the predicted rough spectrum, i.e., Eq. (17)
4. Array 'SPF' is for the predicted smoothed spectrum, i.e., Eq. (18)
5. Array 'FRS' is for the relevant frequency corresponded to 'SPS'
6. Array 'FRF' is for the relevant frequency corresponded to 'SPF'
7. Parameter 'FNU' is for determining the frequency range, i.e., μ in Eq. (7)
8. Parameter 'DT' is for record interval Δt
9. Parameters 'FL' and 'FH' are frequency range, i.e., Eqs. (7) and (8)

10. Subroutine ‘DQDAGS’ is for integrating a function, see Fortran “IMSL Math Library” for more detail
11. Parameter ‘H0’ is for the representative regular wave height
12. Parameter ‘T0’ is for the representative regular wave period

A.3 Subroutine ‘EQU_FRE’

Subroutine “EQU_FRE” is applied to calculate the random wave surface elevation. In which, subroutine “RNSET” and “DRNUN” are used for generating the pseudorandom numbers from a uniform (0, 1) distribution, see Fortran “IMSL Stat Library” for more detail.

1. Array ‘FRE’ is for values at the lateral points of the separated frequencies
2. Arrays ‘WI’ and ‘EPSI’ are for random numbers in range of (0,1)
3. Array ‘SFRE’ is for representative frequency to calculate the component wave amplitude, i.e., f_i in Eq. (3)
4. Array ‘SPE’ is for frequency spectrum at frequency f_i
5. Array ‘FW’ is for the representative frequency, i.e., f_i in Eq. (1)

A.4 Subroutine ‘CORRELATION’

Subroutine “CORRELATION” is applied to calculate the simulated or predicted spectrum. In which, subroutine “DACF” is used for calculating the sample autocorrelation function of a stationary time series, see Fortran “IMSL Stat Library” for more detail.

A.5 Subroutine ‘WAVE_NUM’

Subroutine “WAVE_NUM” is applied to calculate the total number of individual waves in one simulated wave record. In which, subroutine “WAVE_STA” is used for calculating the statistic features of the recorded data. In subroutine “WAVE_STA”, subroutine “DORDST” is for determining the order statistics, see Fortran “IMSL Stat Library” for more detail.

Other subroutines can be easily understood using the information provided in this report together with the further interpretative text in the corresponding parts of the program code.

APPENDIX II – PROGRAM CODE

```
**************************************************************************
C
C       PROGRAM FOR RANDOM WAVE-INDUCED SOIL RESPONSE AND LIQUEFACTION
C
C       HAIJIANG LIU, DONG-SHENG JENG, 2006
C
**************************************************************************
    PROGRAM RANDOM
    USE MSIMSL

    PARAMETER(N=100,NN=1000)
    IMPLICIT DOUBLE PRECISION (A-H,O-Z)
    COMMON/CHA/HS,TS,GAMA
    COMMON/DAT1/D,TKZ,TKXZ,G,U,TNA,SR,H
    COMMON/LIQ/X0,XE,ZE,RS
    COMMON/DSJ/IJ0,IJ1
    COMMON/PAR/PI,RI,RW
    COMMON/SPE/ISPE

    DATA GAMA/3.3/
    CHARACTER CCH
    DIMENSION AMP(N),EPS(N),PER(N),TT(NN)
     DOUBLE COMPLEX RI

   PI=4.0*ATAN(1.0)
   RI=(0.,1.)
   RW=9806.
*******************************************************************************
C   LIST OF DATA FILES
C       'RAN_LIQ.IN'                INPUT DATA FILE
C       'SURFACE.DAT'               SIMULATED RANDOM WAVE SURFACE ELEVATION
C       'SPECTRUM.DAT'              SIMULATED ROUGH FREQUENCY SPECTRUM
C       'SMOOTH_SPECTRUM.DAT'       SIMULATED SMOOTHED FREQUENCY SPECTRUM
C       'REGULAR.DAT'               REGULAR WAVE SOIL RESPONSE
C       'RANDOM.DAT'                RANDON WAVE SOIL RESPONSE
C       'RELATIVE.DAT'              DIFFERENCE BETWEEN REGULAR AND RANDOM WAVE
                                    LOADINGS
*******************************************************************************
    OPEN(1,FILE='RAN_LIQ.IN')
    OPEN(10,FILE='SURFACE.DAT')
    OPEN(11,FILE='SPECTRUM.DAT')
    OPEN(12,FILE='SMOOTH_SPECTRUM.DAT')
    OPEN(20,FILE='REGULAR.DAT')
    OPEN(21,FILE='RANDOM.DAT')
    OPEN(22,FILE='RELATIVE.DAT')
```

```
**********************************
C   INPUT DATA
**********************************
      READ(1,*) ISPE, CCH
      READ(1,*) IJK,  CCH
      READ(1,*) IJ0,  CCH
      READ(1,*) IJ2,  CCH
      READ(1,*) HS,   CCH
      READ(1,*) TS,   CCH
      READ(1,*) D,    CCH
      READ(1,*) TKZ,  CCH
      READ(1,*) TKXZ, CCH
      READ(1,*) G,    CCH
      READ(1,*) U,    CCH
      READ(1,*) TNA,  CCH
      READ(1,*) RS,   CCH
      READ(1,*) SR,   CCH
      READ(1,*) H,    CCH
      READ(1,*) X0,   CCH
      READ(1,*) XE,   CCH
      READ(1,*) ZE,   CCH

      CLOSE(1)

**********************************
C  CALCULATION OF WAVE SPECTRUMS
**********************************
      CALL WSPECTR(AMP,PER,EPS,TT)

      IF (IJK.EQ.0) THEN
**********************************
C  CALCULATION OF WAVE-INDUCED SOIL RESPONSE
**********************************
      CALL SOIL(AMP,PER,TT,EPS)
           ELSE IF(IJK.EQ.1) THEN
****************************************
C  CALCULATION OF LIQUEFACTION DEPTH
****************************************
           CALL LIQUEFACTION(AMP,PER,EPS,TT)
           END IF

      END




****************************************
C   DETERMINATION OF WAVE SPECTRUM
```

```
*****************************************
      SUBROUTINE WSPECTR(AMP,PER,EPS,T)

      PARAMETER(N=100,NN=1000)
      PARAMETER (M=62)

      IMPLICIT DOUBLE PRECISION (A-H,O-Z)
      COMMON/CHA/HS,TS,GAMA
      COMMON/REGULAR/T0,TK0,H0
            COMMON/PAR/PI,RI,RW
            COMMON/SPE/ISPE
      COMMON/DAT1/D,TKZ,TKXZ,G,U,TNA,SR,H
            EXTERNAL FBM,FJONSWAP,SFF2
      DIMENSION T(NN),SUR(NN),PRE(NN),CIGX(NN),CIGZ(NN),TXZ(NN),RPRE(NN)
      DIMENSION AMP(N),EPS(N),PER(N)

C CORRELATION METHOD
      DIMENSION SPS(M+1),SPF(M+1),FRF(M+1),FRS(M+1)

      DOUBLE COMPLEX RI

C  SIGNIFICANT WAVE HEIRHT: HS
C  SIGNIFICANT WAVE PERIOD: TS
C  RANGE OF FREQUENCY: FNU

      FNU=0.002
      DT=1.


*************************************************************
C DETERMINE THE FREQUENCY RANGE
*************************************************************
      IF (ISPE.EQ.1)THEN
C B-M FREQUENCY SPECTRUM
      FL=1./TS*(-1.03/LOG(FNU))**(0.25)
      FH=1./TS*(-1.03/LOG(1.-FNU))**(0.25)
C P-M SPECTRUM
C     FL=(-3.11/HS**2/LOG(FNU))**(0.25)
C     FH=(-3.11/HS**2/LOG(1-FNU))**(0.25)
      ELSE IF(ISPE.EQ.2) THEN
C JONSWAP SPECTRUM
      TP=TS/(1-0.132*(GAMA+0.2)**(-0.559))
      FP=1./TP
      FL=0.*FP
      FH=5.*FP
      END IF
```

```
**********************************************************************
C  CALCULATIION OF BASIC PARAMETERS FOR REPRESENTATIVE REGULAR WAVES
C  H0=HS/SQRT(2.), T0=SQRT(SM0/SM2) ACCORDING TO GODA (2000)
**********************************************************************
      H0=HS/SQRT(2.)

      A=FL
      B=FH

      ERRABS = 0.0
      ERRREL = 0.001

      IF (ISPE.EQ.1) THEN
C  B-M SPECTRUM
      CALL DQDAGS (FBM, A, B, ERRABS, ERRREL, SM0, ERREST)
      ELSE IF(ISPE.EQ.2) THEN
C  JONSWAP SPECTRUM
      CALL DQDAGS (FJONSWAP, A, B, ERRABS, ERRREL, SM0, ERREST)
      END IF
      CALL DQDAGS (SFF2, A, B, ERRABS, ERRREL, SM2, ERREST)

            T0=DSQRT(SM0/SM2)
            WRITE(*,*) 'REPRESENTATIVE WAVE HEIGHT =',H0
            WRITE(*,*) 'REPRESENTATIVE WAVE PERIOD =',T0

      CALL WAVEL(D,T0,TL0)
      TK0=2*PI/TL0

**************************************************************
C EQUALLY SEPARATE THE FREQUENCY FOR RANDOM WAVE SIMULATION
**************************************************************
      CALL EQU_FRE(N,NN,FL,FH,DT,T,SUR,AMP,PER,EPS)

      SURM=SUM(SUR)/DBLE(NN)
      DO I=1,NN
       SUR(I)=SUR(I)-SURM
       WRITE(10,*) T(I),SUR(I)
      END DO

      CALL WAVE_NUM(NN,DT,T,SUR)

C  USING CORRELATION FUNCTION
      CALL CORRELATION(NN,M,SUR,FRS,SPS,FRF,SPF,PI,DT)
      DO I=1,M+1
       WRITE(11,*) FRS(I),SPS(I)*2*PI
       WRITE(12,*) FRF(I),SPF(I)*2*PI
      END DO
```

```
      CLOSE(10)
      CLOSE(11)
      CLOSE(12)

      RETURN
      END



*****************************************************************
C CORRELATION METHOD FOR SPECTRUM ESTIMATION
*****************************************************************
      SUBROUTINE CORRELATION(NN,M,SUR,FRS,SPS,FRF,SPF,PI,DT)
      IMPLICIT DOUBLE PRECISION (A-H,O-Z)
      DIMENSION SUR(NN),FRS(M+1),SPS(M+1),FRF(M+1),SPF(M+1)
      DIMENSION COR(M+1),ACV(M+1),AC(M+1),SEAC(M+1)

      DO I=1,M+1
       FRS(I)=DBLE(I-1)/M/2./DT
       FRF(I)=FRS(I)
      END DO

      NOBS=NN
      INPRINT=0
      ISEOPT=0
      IMEAN=1
      MAXLAG=M

      CALL DACF(NOBS,SUR,INPRINT,ISEOPT,IMEAN,XMEAN,MAXLAG,ACV,AC,SEAC)

      DO I=1,M+1
       COR(I)=ACV(I)*NOBS/(NOBS-(I-1))
      END DO

      DO I=1,M+1
       SM=0.
       DO J=2,M
        SM=SM+COR(J)*COS(2*PI*FRF(I)*DT*(J-1))
       END DO

       SPS(I)=2.*DT/PI*(0.5*COR(1)+
     1       0.5*COR(M+1)*COS(2*PI*FRF(I)*DT*M)+SM)

      END DO

      SPF(1)=0.54*SPS(1)+0.46*SPS(2)
      SPF(M+1)=0.46*SPS(M)+0.54*SPS(M+1)
```

```
      DO I=2,M
       SPF(I)=0.23*SPS(I-1)+0.54*SPS(I)+0.23*SPS(I+1)
      END DO

      END



**********************************************************************
C CALCULATION OF INDIVIDUAL WAVE NUMBERS IN ONE RANDOM WAVE RECORD
**********************************************************************
      SUBROUTINE WAVE_NUM(NN,DT,T,SUR)
      IMPLICIT DOUBLE PRECISION (A-H,O-Z)
      DIMENSION T(NN),SUR(NN)
      DIMENSION TS(NN),HS(NN)

      DO I=1,NN
       IF(SUR(I)*SUR(I+1).LT.0..AND.SUR(I+1).GT.0.) THEN
       ISTA=I
       GOTO 200
       END IF
      END DO

200   NWAVE=0

300   DO J=ISTA+1,NN-1

        IF(SUR(J)*SUR(J+1).LT.0..AND.SUR(J+1).GT.0.) THEN
          IEND=J
          GOTO 100
        ELSE
         IF(J.EQ.NN-1) GOTO 400
        END IF
      END DO

100     NWAVE=NWAVE+1
        TSTART=T(ISTA+1)-
     1       SUR(ISTA+1)/(SUR(ISTA+1)-SUR(ISTA))*(T(ISTA+1)-T(ISTA))
        TEND=T(IEND+1)-
     1       SUR(IEND+1)/(SUR(IEND+1)-SUR(IEND))*(T(IEND+1)-T(IEND))
        TS(NWAVE)=TEND-TSTART

        DO II=ISTA+1,IEND
         IF (SUR(II).GT.SUR(II-1).AND.SUR(II).GT.SUR(II+1)) THEN
          CA=0.5*(SUR(II-1)-2.*SUR(II)+SUR(II+1))
          CB=0.5*(SUR(II+1)-SUR(II-1))
```

```
        CC=SUR(II)
        HMAX=CC-CB**2/4./CA
       END IF
       IF (SUR(II).LT.SUR(II-1).AND.SUR(II).LT.SUR(II+1)) THEN
        CA=0.5*(SUR(II-1)-2.*SUR(II)+SUR(II+1))
        CB=0.5*(SUR(II+1)-SUR(II-1))
        CC=SUR(II)
        HMIN=CC-CB**2/4./CA
       END IF
      END DO
      HS(NWAVE)=HMAX-HMIN

      IF (IEND.EQ.NN-1) THEN
       GOTO 400
      ELSE
       ISTA=IEND
       GOTO 300
      END IF

400   WRITE(*,*) 'TOTAL NUMBER OF WAVES =', NWAVE

C  NP=1:      MEAN WAVE HIGHT
C  NP=3:      1/3 WAVE HIGHT (SIGNIFICANT WAVE HIGHT)
C  NP=10:     1/10 WAVE HIGHT
C  NP=NWAVE:  HIGHEST WAVE HIGHT
      NP=1
      NOBS=NWAVE
      NOS=NWAVE/NP
      IOPT=2
      CALL WAVE_STA(NN,NWAVE,HS,TS,NP,NOBS,NOS,IOPT)

      END



************************************************************
C STATISTICS FEATURES OF THE SIMULATED RANDOM WAVES
************************************************************
      SUBROUTINE WAVE_STA(NN,NWAVE,HS,TS,NP,NOBS,NOS,IOPT)
      IMPLICIT DOUBLE PRECISION (A-H,O-Z)
      DIMENSION HS(NN),TS(NN)
      DIMENSION IOS(1),OSH(NOS),OST(NOS)

      CALL DORDST (NOBS, HS, NOS, IOPT, IOS, OSH, NMISS)

      DO J=1,NOS
       DO I=1,NWAVE
```

```
      IF(HS(I).EQ.OSH(J)) OST(J)=TS(I)
     END DO
    END DO

    AVEH=SUM(OSH)/NOS
    AVET=SUM(OST)/NOS

    WRITE(*,*) 'THE 1/',NP,' WAVE HIGHT =', AVEH
    WRITE(*,*) 'THE 1/',NP,' WAVE PERIOD =', AVET

    END



**********************************************************************
C EQUALLY SEPARATE THE FREQUENCY FOR RANDOM WAVE SIMULATION
**********************************************************************
    SUBROUTINE EQU_FRE(N,NN,FL,FH,DT,T,SUR,AMP,PER,EPS)
    IMPLICIT DOUBLE PRECISION (A-H,O-Z)
    COMMON/SPE/ISPE
    COMMON/DAT1/D,TKZ,TKXZ,G,U,TNA,SR,H
    COMMON/LIQ/X0,XE,ZE,RS
    COMMON/REGULAR/T0,TK0,H0
    COMMON /CHA/ HS,TS,GAMA

    DIMENSION T(NN),SUR(NN)
    DIMENSION FRE(N+1),WI(N),EPSI(N),AMP(N),PER(N)
    DIMENSION SFRE(N),SPE(N),FW(N),EPS(N)

    EXTERNAL FBM,FJONSWAP

    PI=ACOS(-1.)

    TL0=2*PI/TK0
    XX=X0*TL0

    DF=(FH-FL)/N

    DO I=1,N+1
     FRE(I)=FL+(I-1)*DF
    END DO

    NR=N
    ISEED=1234567
    CALL RNSET(ISEED)
    CALL DRNUN(NR,WI)
    CALL DRNUN(NR,EPSI)
```

```
      DO I=1,N
       SFRE(I)=(FRE(I)+FRE(I+1))/2.
       IF(ISPE.EQ.1) THEN
CC B-M SPECTRUM
        SPE(I)=FBM(SFRE(I))
       ELSE IF(ISPE.EQ.2) THEN
CC JONSWAP SPECTRUM
       SPE(I)=FJONSWAP(SFRE(I))
       END IF
       FW(I)=FRE(I)+(FRE(I+1)-FRE(I))*WI(I)
       EPS(I)=2.*PI*EPSI(I)
      END DO

      DO J=1,NN
       T(J)=J*DT
       SUR(J)=0.
       DO I=1,N
        AMP(I)=DSQRT(2.*SPE(I)*DF)
        PER(I)=1./FW(I)

             CALL WAVEL(D,PER(I),WL)
             TK=2*PI/WL
        SUR(J)=SUR(J)+AMP(I)*COS(TK*XX-2.*PI*FW(I)*T(J)+EPS(I))
       END DO

      END DO

      END



*****************************************************************
C   B_M SPECTRUM
*****************************************************************
      FUNCTION FBM(F)
      IMPLICIT DOUBLE PRECISION (A-H,O-Z)
      COMMON /CHA/ HS,TS,GAMA
      FBM=0.257*HS**2*TS**(-4)*F**(-5)*DEXP(-1.03*(TS*F)**(-4))
      RETURN
      END



*****************************************************************
C   JONSWAP SPECTRUM
*****************************************************************
      FUNCTION FJONSWAP(F)
```

```
      IMPLICIT DOUBLE PRECISION (A-H,O-Z)
      COMMON /CHA/ HS,TS,GAMA

      TP=TS/(1-0.132*(GAMA+0.2)**(-0.559))
      FP=1./TP
       IF (F.LE.FP)   THEN
        SIGMA=0.07
       ELSE
        SIGMA=0.09
       END IF
       BETAJ=0.0624*(1.094-0.01915*DLOG(GAMA))/
     1     (0.230+0.0336*GAMA-0.185/(1.9+GAMA))
       FJONSWAP=BETAJ*HS**2*TP**(-4)*F**(-5)*
     1       DEXP(-1.25*(TP*F)**(-4))*
     2       GAMA**(DEXP(-(TP*F-1)**2/2/SIGMA**2))
       RETURN
       END



************************************************************
C FOR 2ND-SPECTRAL MOMENT SM2
************************************************************
      FUNCTION SFF2(F)
      IMPLICIT DOUBLE PRECISION (A-H,O-Z)
      COMMON/SPE/ISPE

      EXTERNAL FBM,FJONSWAP

            IF (ISPE.EQ.1) SFF2=F*F*FBM(F)
            IF(ISPE.EQ.2) SFF2=F*F*FJONSWAP(F)

       RETURN
       END



************************************************************
C   DETERMINATION OF WAVELENGTH (HUNT'S FORMULA)
************************************************************
      SUBROUTINE WAVEL(D,T,TL)
      IMPLICIT DOUBLE PRECISION (A-H,O-Z)
      PI=4.0*ATAN(1.0)
      W=2*PI/T
      G1=9.806
      GD1=0.6666666667
      GD2=0.3555555556
```

```
      GD3=0.1608465608
      GD4=0.0632098765
      GD5=0.0217540484
      GD6=0.0065407983
      WD=W*W*D/G1
      FA=1+GD1*WD+GD2*WD*WD+GD3*WD**3+GD4*WD**4+GD5*WD**5+GD6*WD**6
      FF=WD*WD+WD/FA
      TL=SQRT(4*PI*PI*D*D/FF)
      RETURN
      END



*********************************************************
C  SOIL RESPONSE
*********************************************************
      SUBROUTINE SOIL(AMP,PER,T,EPS)

      PARAMETER(N=100,NN=1000)
      IMPLICIT DOUBLE PRECISION (A-H,O-Z)
      COMMON/DAT1/D,TKZ,TKXZ,G,U,TNA,SR,H
      COMMON/LIQ/X0,XE,ZE,RS
      COMMON/DAT4/C1,C2,C3,C4,C5,C6,DA,S
      COMMON/REGULAR/T0,TK0,H0
      COMMON/CHA/HS,TS,GAMA
      COMMON/SRES/PORE,CIGX,CIGZ,TXZ
      COMMON/PAR/PI,RI,RW
       COMMON/DSJ/IJ0,IJ1

      DOUBLE COMPLEX RI,DA,SDS,C1,C2,C3,C4,C5,C6,EXT,PORE,
     & CIGX,CIGZ,TXZ,S
      DIMENSION T(NN),AMP(N),EPS(N),PER(N)
      CHARACTER*25 FNAME

C **********************************
C  REGULAR WAVES
C **********************************
      TL0=2*PI/TK0
      AMP0=H0/2
      W0=2*PI/T0

            H=4.0*D
c           Z=-ZE*H
      XX=X0*TL0

            NZ=50
```

```
            DO IZ=1,NZ+1
             IF(IJ0.EQ.0) Z=-(IZ-1.)*H/NZ
             IF(IJ0.EQ.1) Z=-(IZ-1.)*H/NZ

            CALL COEF(T0)
          CALL SP(AMP0,TK0,W0,Z,PB0)
          PORER=ABS(PORE)/RW/D
          CIGXR=ABS(CIGX)/RW/D
          CIGZR=ABS(CIGZ)/RW/D
          TXZR=ABS(TXZ)/RW/D

c           WRITE(*,*) Z,PORER,CIGXR,CIGZR,TXZR
            IF(IJ0.EQ.0) WRITE(20,1021) PORER,CIGXR,CIGZR,TXZR,Z/H
            IF(IJ0.EQ.1) WRITE(20,1021) PORER,CIGXR,CIGZR,TXZR,Z/H

C **********************************
C  RANDOM WAVES
C **********************************

C     Z=-ZE*TL0
C     XX=X0*TL0
          PMAX=-1000.
            CXMAX=-1000.
            CZMAX=-1000.
            TMAX=-1000.

          DO I=1,NN
           POREIR=0.
           CIGXIR=0.
           CIGZIR=0.
           TXZIR=0.

            DO J=1,N
             CALL WAVEL(D,PER(J),WL)
             W=2*PI/PER(J)
             TK=2*PI/WL
             EXT=EXP(RI*(TK*XX-W*T(I)+EPS(J)))
             CALL COEF(PER(J))
             CALL SP(AMP(J),TK,W,Z,PB)
C             WRITE(*,*) PORE
             POREIR=POREIR+REAL(PORE*EXT)/RW/D
             CIGXIR=CIGXIR+REAL(CIGX*EXT)/RW/D
             CIGZIR=CIGZIR+REAL(CIGZ*EXT)/RW/D
             TXZIR=TXZIR+REAL(TXZ*EXT)/RW/D
            END DO
            IF(POREIR.GT.PMAX) PMAX=POREIR
            IF(CIGXIR.GT.CXMAX) CXMAX=CIGXIR
```

```
            IF(CIGZIR.GT.CZMAX) CZMAX=CIGZIR
            IF(TXZIR.GT.TMAX) TMAX=TXZIR
C       WRITE(21,1021) T(I),POREIR,CIGXIR,CIGZIR,TXZIR
      END DO

            IF(IJ0.EQ.0) WRITE(21,1021) PMAX,CXMAX,CZMAX,TMAX,Z/H
            IF(IJ0.EQ.1) WRITE(21,1021) PMAX,CXMAX,CZMAX,TMAX,Z/H
            RELP=(PMAX-PORER)
            RELCX=(CXMAX-CIGXR)
            RELCZ=(CZMAX-CIGZR)
            RELT=(TMAX-TXZR)
            IF(IJ0.EQ.0) WRITE(22,1021) RELP,RELCX,RELCZ,RELT,Z/H
            IF(IJ0.EQ.1) WRITE(22,1021) RELP,RELCX,RELCZ,RELT,Z/H

            WRITE(*,*) IZ,Z
            END DO


1021      FORMAT(2X,5(E12.6,',',2X))
            RETURN
            END



*****************************************************************
C   CALCULATION OF COEFFICIENTS FOR SOIL RESPONSE
*****************************************************************
      SUBROUTINE COEF(PER)

      IMPLICIT DOUBLE PRECISION (A-H,O-Z)

      COMMON/DAT1/D,TKZ,TKXZ,G,U,TNA,SR,H
      COMMON/LIQ/X0,XE,ZE,RS
      COMMON/DAT4/C1,C2,C3,C4,C5,C6,DA,S
      COMMON/DSJ/IJ0,IJ1
      COMMON/PAR/PI,RI,RW
      DOUBLE COMPLEX RI,DA,SDS,A1,A2,A3,A4,A5,A6,A7,A8,A9,
     1 A10,A11,A12,A13,A14,A15,A16,A17,A18,A19,A20,A21,A22,A23,
     2 A24,C00,C01,C02,C03,C04,C05,C06,C07,C10,C11,C12,C13,C14,
     3 C15,C16,C17,C20,C21,C22,C23,C24,C25,C26,C27,C30,C31,C32,
     4 C33,C34,C35,C36,C37,C40,C41,C42,C43,C44,C45,C46,C47,C50,
     5 C51,C52,C53,C54,C55,C56,C57,C60,C61,C62,C63,C64,C65,C66,
     6 C67,D0,D1,D2,D3,D4,D5,D6,C1,C2,C3,C4,C5,C6,EKDH,E4K2DH,
     7    E2DH,E2K2DH,E3KDH,S1,S2,S,SA,EDX,CXY,EDZ,DA2,DA3,DA4,DA5

*****************************************************
C    ASSIGN PARAMETERS
```

```
*******************************************************
      TKW=2.0E9
*******************************************************
C     INPUT DATA
*******************************************************
      T=PER
      W=2*PI/T
*******************************************************
C     CALCULATE WAVE LENGTH (HUNT'S FORMULA)
*******************************************************
      DEPTH=D
      CALL WAVEL(DEPTH,T,TL)
      TK=2.0*PI/TL
C     WRITE(*,*) TL
*******************************************************
C     CALCULATE BASIC PARAMETERS
*******************************************************
      B=1./TKW+(1.-SR)/(RW*D)
      IF(SR .EQ. 1.0) B=0.0
      GB=G*B

      TK2=TK**2
      TK3=TK**3
      TK4=TK**4
      TK5=TK**5
      TK6=TK**6
      SDS=TK2*TKXZ-RI*RW*W*(TNA*GB+(1-2*U)/(2-2*U))/(TKZ*G)
      DA=SQRT(SDS)
      S1=TK2*(1-TKXZ)+RI*W*RW*TNA*GB/(G*TKZ)
      S2=TK2*(1-TKXZ)+RI*W*RW*(TNA*GB+1-2*U)/(G*TKZ)
      S=S1*(1-2*U)/S2
      SA=1-S
      DA2=DA**2
      DA3=DA**3
      DA4=DA**4
      DA5=DA**5

*******************************************************
C     CALCUALTE COEFFICIENTS
*******************************************************
      A1=TK2*U-(1-U)*(DA2+DA*TK+TK2)
      A2=-DA2+DA*TK-TK2+DA2*U-DA*TK*U+2*TK2*U
      A3=(1-U)*(DA3*H-TK2-DA*TK2*H)+TK2*U
      A4=(1-U)*(DA3*H+TK2-DA*TK2*H)-TK2*U
      A5=2*DA*TK*H*(DA-TK)*(1-U)
      A6=2*DA*TK*H*(DA+TK)*(1-U)
      A7=-2*DA*(DA+TK)*(1-U)+TK2
```

```
      A8=4*TK6*H*(1-U)+4*DA*TK4*(1-4*U+U*U-S*(3-3*U+U*U))+
     1    4*DA3*TK2*(2+S*(3-2*U))*(1-U)-4*DA4*TK2*H*(1-U)-
     2    4*DA5*(1+S)*(1-U)*(1-U)
      A9=-DA2*(1-U)+TK2*(2-U)
      A10=-2*DA*(DA-TK)*(1-U)+TK2
      A11=TK5*(SA-2*U)-2*TK6*H*U-
     1     DA2*TK3*(1-U)*(1+2*TK*H*(1-2*U)+TK*S*(5-4*U))+
     2     2*DA4*TK*(1-U)*(1-U)*(1+2*TK*H+2*S)
      A12=DA*TK4*(2*TK*H*(1-U-U*U)+S*(2+U-2*U*U)-
     1     (2-6*U+3*U*U))-DA3*TK2*(1-U)*(2*TK*H+3*S+2*U)+
     2      DA5*(1-U)*(1-U)*(1+2*TK*H+2*S)
      A13=2*TK4*DA*(TK*H*(3-5*U+4*U*U)-
     1     S*(5-10*U+4*U*U)-U*(3-4*U))+TK2*DA3*(1-U)*((3-4*U)-
     2       2*TK*H*(5-4*U)+2*S*(1-2*U))
      A14=-TK4*(SA-2*U)-2*DA2*TK2*(2-U)*(1-U)+
     1        2*DA4*(1-U)*(1-U)
      A15=DA*TK3*(S+U)*(3-2*U)+DA3*TK*(1-U)*(1-2*S-2*U)
      A16=-2*DA*TK2*(DA2*(1-U)*(1+4*U)+TK2*(3-11*U+4*U*U))
      A17=TK4*U*(SA-2*U)+2*DA*TK4*H*(1-U-U*U)-
     1      DA2*TK2*(1-U)*(1+S*(5-4*U))-2*DA3*TK2*H*(1-U)+
     2      2*DA4*(1+2*S)*(1-U)*(1-U)+2*DA5*H*(1-U)*(1-U)
      A18=-TK4*U*(SA-2*U)+2*DA*TK4*H*(1-U-U*U)+
     1        DA2*TK2*(1-U)*(1+S*(5-4*U))-2*DA3*TK2*H*(1-U)-
     2        2*DA4*(1+2*S)*(1-U)*(1-U)+2*DA5*H*(1-U)*(1-U)
      A19=-DA2*(1-U)*(3-4*U+2*S*(1-2*U))+
     1              TK2*((3-4*U)*U+S*(5-10*U+4*U*U))
      A20=A14
      A21=-A15
      A22=DA*A19
      A23=-DA*(DA+2*TK)*(1-U)+TK2*U
      A24=-DA*(DA-2*TK)*(1-U)+TK2*U
      C00=(DA-TK)*(DA-TK)*(DA+TK*S-DA*U+TK*U)*(A1+S*A7)
      C01=-2*DA*((TK2*U-DA2+DA2*U)**2+TK4*(1-2*U)**2+
     1          2*TK2*H*H*(1-U)*(1-U)*(DA2-TK2)**2)+
     2          4*TK2*H*(DA4-TK4)*(1-U)*(1-2*U)+S*A8
      C02=-8*DA*TK2*(SA-2*U)*(TK*H*(DA2-TK2)*(1-U)-
     1             DA2*(1-U)+TK2*U+S*A9)
      C03=(DA+TK)*(DA+TK)*(DA-DA*U-TK*U-TK*S)*(A2+S*A10)
      C04=C03
      C05=C01-8*TK2*H*(DA4-TK4)*(1-U)*(SA-2*U)
      C06=C02+16*DA*TK3*H*(DA2-TK2)*(1-U)*(SA-2*U)
      C07=C00
      C10=-(DA-TK)*S*(-DA*(DA-2*TK)*(1-U)+TK2*U)*(A1+S*A7)
      C11=2*TK2*H*(DA+TK)*(DA-DA*U-TK*U)*A3+S*(A11+A12)
      C12=4*DA*TK3*H*(1-2*U)*(DA2-DA2*U-TK2*U)+S*A13
      C13=0.0
      C14=S*(DA+TK)*(DA*(DA+2*TK)*(1-U)-TK2*U)*(A2+S*A10)
```

```
      C15=2*TK2*H*(DA-TK)*(DA-DA*U+TK*U)*A4+S*(A12-A11)
      C16=2*DA*TK2*S*((1-U)*(DA2*(1+2*S)+TK*H*(DA2-TK2))+
     1               TK2*(2*S*U-3*S-U))
      C17=0.0
      C20=(DA-TK)*(DA-TK)*(DA-DA*U+TK*U)*(A1+S*A7)
      C21=C03+(DA+TK)*(S*(A14+A15)+(DA+TK)*(DA-DA*U-TK*U)*A5)
      C22=4*DA*TK2*(1-2*U)*(2*DA2*(1-U)-2*TK2*U-
     1                 TK*H*(1-U)*(DA2-TK2))+S*A16
      C23=0.0
      C24=(DA+TK)*(DA+TK)*(DA-DA*U-TK*U)*(A2+S*A10)
      C25=C00+(DA-TK)*(S*(A14-A15)+(DA-TK)*(DA-DA*U+TK*U)*A6)
      C26=2*DA*TK2*S*(DA2-TK2)*(1-U)
      C27=0.0
      C30=0.0
      C31=2*TK2*H*(DA-TK)*(DA-DA*U+TK*U)*A3+S*(A11+A12-2*TK*A17)
      C32=-2*DA2*TK*S*((TK*H-S)*(DA2-TK2)*(1-U)-DA2*(1-U)+
     1               TK2*U+S*A9)
      C33=C14
      C34=0.0
      C35=2*TK2*H*(DA+TK)*(DA-DA*U-TK*U)*A4+S*(A12-A11-2*TK*A18)
      C36=-C12-4*DA*TK2*S*A19
      C37=C10
      C40=0.0
      C41=C25-2*C00-2*S*(DA-TK)*(A20+A21)
      C42=-C26
      C43=-C24
      C44=0.0
      C45=C21-2*C03-2*S*(DA+TK)*(A20-A21)
      C46=4*DA*TK2*(1-2*U)*(2*TK2*U-2*DA2*(1-U)-
     1                 TK*H*(1-U)*(DA2-TK2))-S*A16
      C47=-C20
      C50=S*(DA-TK)*(A1+S*A7)
      C51=-4*TK2*H*(1-2*U)*A3+2*S*(-2*TK4*H*(1-2*U)+A22)
      C52=-2*TK*(SA-2*U)*(TK*H*(DA+TK)*(DA-DA*U-TK*U)+S*A23)
      C53=S*(DA+TK)*(A2+S*A10)
      C54=0.0
      C55=0.0
      C56=2*TK*(SA-2*U)*(-TK*H*(DA-TK)*(DA-DA*U+TK*U)+S*A24)
      C57=0.0
      C60=0.0
      C61=0.0
      C62=-C56+4*TK*S*(SA-2*U)*A24
      C63=0.0
      C64=C53
      C65=-4*TK2*H*(1-2*U)*A4+2*S*(2*TK4*H*(1-2*U)+A22)
      C66=-C52-4*TK*S*(SA-2*U)*A23
      C67=C50
```

```
      E2KH=EXP(-2*TK*H)
      E4KH=EXP(-4*TK*H)
      EKDH=EXP(-(TK+DA)*H)
      E2K2DH=EXP(-2*(TK+DA)*H)
      E3KDH=EXP(-(3*TK+DA)*H)
      E4K2DH=EXP(-(4*TK+2*DA)*H)
      E2DH=EXP(-2*DA*H)
      IF(IJ0 .EQ. 0) THEN
       E2KH=0.0
       E4KH=0.0
       EKDH=(0.0,0.0)
       E2K2DH=(0.0,0.0)
       E3KDH=(0.0,0.0)
       E4K2DH=(0.0,0.0)
       E2DH=(0.0,0.0)
      ENDIF
      D0=C00+C01*E2KH+C02*EKDH+C03*E4KH+C04*E2DH+C05*E2K2DH+
     1          C06*E3KDH+C07*E4K2DH
      D1=C10+C11*E2KH+C12*EKDH+C13*E4KH+C14*E2DH+C15*E2K2DH+
     1          C16*E3KDH+C17*E4K2DH
      D2=C20+C21*E2KH+C22*EKDH+C23*E4KH+C24*E2DH+C25*E2K2DH+
     1          C26*E3KDH+C27*E4K2DH
      D3=C30+C31*E2KH+C32*EKDH+C33*E4KH+C34*E2DH+C35*E2K2DH+
     1          C36*E3KDH+C37*E4K2DH
      D4=C40+C41*E2KH+C42*EKDH+C43*E4KH+C44*E2DH+C45*E2K2DH+
     1          C46*E3KDH+C47*E4K2DH
      D5=C50+C51*E2KH+C52*EKDH+C53*E4KH+C54*E2DH+C55*E2K2DH+
     1          C56*E3KDH+C57*E4K2DH
      D6=C60+C61*E2KH+C62*EKDH+C63*E4KH+C64*E2DH+C65*E2K2DH+
     1          C66*E3KDH+C67*E4K2DH
      C1=D1/D0
      C2=D2/D0
      C3=D3/D0
      C4=D4/D0
      C5=D5/D0
      C6=D6/D0

      RETURN
      END



*******************************************
C     CALCULATE SOIL RESPONSE VARIABLES
*******************************************
      SUBROUTINE SP(AMP,TK,W,Z,PB)
      IMPLICIT DOUBLE PRECISION (A-H,O-Z)
```

```
      COMMON/DAT1/D,TKZ,TKXZ,G,U,TNA,SR,H
      COMMON/LIQ/X0,XE,ZE,RS
      COMMON/DAT4/C1,C2,C3,C4,C5,C6,DA,S
      COMMON/SRES/PORE,CIGX,CIGZ,TXZ
      COMMON/PAR/PI,RI,RW

      DOUBLE COMPLEX RI,DA,S,SA,C1,C2,C3,C4,C5,C6,EDK,EDX,PORE,
     & CIGX,CIGZ,TXZ,DA2


      HS=2*AMP
      CH=0.5*(EXP(TK*D)+1./EXP(TK*D))
      PB=0.5*RW*HS/CH
      SA=1-S

      TK2=TK*TK
      DA2=DA*DA

      EKZ=EXP(TK*Z)
      EDZ=EXP(DA*Z)
      EKX=EXP(-TK*Z)
      IF(ABS(EDZ) .LE. 1.0E-20) THEN
       EDX=1.0E20
      ELSE
       EDX=EXP(-DA*Z)
      ENDIF

      PORE=PB*(((SA-2*U)*(C2*EKZ-C4*EKX)+
     1      (1-U)*(DA2-TK2)*(C5*EDZ+C6*EDX))/(1-2*U))
      CIGX=-PB*(((C1+C2*TK*Z)+2*S*U*C2/(1-2*U))*EKZ+
     1       ((C3+C4*TK*Z)-2*S*U*C4/(1-2*U))*EKX+
     1       (TK2-U*(DA2-TK2)/(1-2*U))*(C5*EDZ+C6*EDX))
      CIGZ=PB*((C1+C2*TK*Z-2*S*(1-U)*C2/(1-2*U))*EKZ+
     1        (C3+C4*TK*Z+2*S*(1-U)*C4/(1-2*U))*EKX+
     1        (DA2*(1-U)-TK2*U)*(C5*EDZ+C6*EDX)/(1-2*U))
      TXZ=PB*RI*((C1+(TK*Z-S)*C2)*EKZ-(C3+(TK*Z+S)*C4)*EKX+
     1         TK*DA*(C5*EDZ-C6*EDX))

      RETURN
      END



**********************************************************************
C SOIL LIQUEFACTION
**********************************************************************
      SUBROUTINE LIQUEFACTION(AMP,PER,EPS,T)
```

```
      PARAMETER (N=100,NN=1000)
      implicit double precision (a-h,o-z)
     COMMON/REGULAR/T0,TK0,H0
     COMMON/LIQ/X0,XE,ZE,RS
     COMMON/DAT1/D,TKZ,TKXZ,G,U,TNA,SR,H
           DIMENSION T(NN),AMP(N),PER(N),EPS(N)

*****************************************************************
C          'RAN_LIQ.DAT'          LIQUEFACTION DEPTH OF RANDOM WAVES
C          'REG_LIQ.DAT'          LIQUEFACTION DEPTH OF REGULAR WAVES
*****************************************************************
           OPEN(30,FILE='RAN_LIQ.DAT')
           OPEN(31,FILE='REG_LIQ.DAT')

           NSR=25
           DO ISR=1,NSR+1
           SR=0.95+(ISR-1)*0.05/NSR

************************
C REGULAR WAVE
************************
           CALL REG_LIQ(ZMIN0)
           WRITE(*,*) 'REGUALR',ZMIN0
************************
C RANDOM WAVE
************************
           ZMIN=1000.
           DO IT=1,NN
     ft=1.0e-3
     z1=-0.0001
     z2=-ze
     call dsj3(AMP,PER,EPS,z1,f1,T(IT))
     call dsj3(AMP,PER,EPS,z2,f2,T(IT))
     f12=f2*f1
     if(f12 .gt. 0.0) then
      zr=0.0
      GOTO 100
     endif

     do i=1,10000
           zerr=abs(z2-z1)/2.
     if(zerr .le. ft) GOTO 100

     zr=z2-f2*(z2-z1)/(f2-f1)
     call dsj3(AMP,PER,EPS,zr,fr,T(IT))
     if(abs(fr) .le. ft) GOTO 100
     if (fr*f1 .gt. 0.0) then
```

```
      z1=zr
      f1=fr
     else
      z2=zr
      f2=fr
     endif
     if (i. eq. 10000 ) then
      write(*,*) i,zr,z1,z2,fr,f1,f2
      pause
     endif
     enddo

100   WRITE(*,*) IT,ISR
     IF(ZR.LT.ZMIN) ZMIN=ZR
          END DO


          WRITE(30,*) SR,ABS(ZMIN)
          WRITE(31,*) SR,ABS(ZMIN0)
          END DO

          CLOSE(30)
          CLOSE(31)
     RETURN
     END



**********************************************************************
C SOIL LIQUEFACTION CRITERIA OF DONG (1997) FOR RANDOM WAVES
**********************************************************************
     SUBROUTINE DSJ3(AMP,PER,EPS,Z,F,T)
     PARAMETER (N=100,NN=1000)
     implicit double precision (a-h,o-z)
     COMMON/CHA/HS,TS,GAMA
     COMMON/DAT1/D,TKZ,TKXZ,G,U,TNA,SR,H
     COMMON/LIQ/X0,XE,ZE,RS
     COMMON/REGULAR/T0,TK0,H0
     COMMON/DAT4/C1,C2,C3,C4,C5,C6,DA,S
     COMMON/SRES/PORE,CIGX,CIGZ,TXZ
     COMMON/PAR/PI,RI,RW

     double complex c1,c2,c3,c4,c5,c6,da,s,cxy,ri,PORE,
          1          CIGX,CIGZ,TXZ,EXT

          DIMENSION PER(N),EPS(N),AMP(N)
```

```
      OK=u/(1.-u)
    TL0=2*PI/TK0
    XX=X0*TL0

      FT=0.

      DO I=1,N
       CALL WAVEL(D,PER(I),WL)
       W=2*PI/PER(I)
       TK=2*PI/WL
       EXT=EXP(RI*(TK*XX-W*T+EPS(I)))
       CALL COEF(PER(I))
       CALL SP(AMP(I),TK,W,Z,PB)
       FT=FT+REAL((PB-PORE)*EXT)
      END DO

    F=-(rs-1.)*(1+2*ok)*rw*z/3.0+FT

      RETURN
      END



**************************************************
C REGULAR WAVE LIQUEFACTION
**************************************************
    SUBROUTINE REG_LIQ(ZMIN)
    PARAMETER (NT=100)
    implicit double precision (a-h,o-z)
    COMMON/LIQ/X0,XE,ZE,RS
      OPEN(2,FILE='TEMP.DAT')

      TTB=0.
      TTE=1.

      ZMIN=1000.
      DO IT=1,NT
       TT=TTB+(IT-1.)*(TTE-TTB)/(NT-1.)
    ft=1.0e-3
    z1=-0.0001
    z2=-ze
    call dsj30(z1,f1,TT)
    call dsj30(z2,f2,TT)
    f12=f2*f1
    if(f12 .gt. 0.0) then
     zr=0.0
     GOTO 100
```

```
      endif

      do i=1,10000
      zr=z2-f2*(z2-z1)/(f2-f1)
      call dsj30(zr,fr,TT)
      zerr=abs(z2-z1)/2.
      if(zerr .le. ft) then
       GOTO 100
      endif
      if(abs(fr) .le. ft) then
       GOTO 100
      endif
      if (fr*f1 .gt. 0.0) then
       z1=zr
       f1=fr
      else
       z2=zr
       f2=fr
      endif
      if (i. eq. 10000 ) then
       write(*,*) i
       pause
      endif
      enddo

100   IF(ZR.LT.ZMIN) ZMIN=ZR
            WRITE(2,*) TT,ZR

            END DO
      RETURN
      END



**********************************************************************
C  SOIL LIQUEFACTION CRITERIA OF DONG (1997) FOR REGULAR WAVES
**********************************************************************
      SUBROUTINE DSJ30(Z,F,T)
      implicit double precision (a-h,o-z)
      COMMON/CHA/HS,TS,GAMA
      COMMON/DAT1/D,TKZ,TKXZ,G,U,TNA,SR,H
      COMMON/LIQ/X0,XE,ZE,RS
      COMMON/REGULAR/T0,TK0,H0
      COMMON/DAT4/C1,C2,C3,C4,C5,C6,DA,S
      COMMON/SRES/PORE,CIGX,CIGZ,TXZ
      COMMON/PAR/PI,RI,RW
```

```
      double complex c1,c2,c3,c4,c5,c6,da,s,cxy,ri,PORE,
     1            CIGX,CIGZ,TXZ,EXT

      OK=U/(1.-U)
    XX=X0

      AMP0=H0/2.
      W0=2*PI/T0

      EXT=EXP(RI*(2*PI*XX-2*PI*T))
      CALL COEF(T0)
    CALL SP(AMP0,TK0,W0,Z,PB0)

    F=-(rs-1.)*(1+2*ok)*rw*z/3.0+REAL((PB0-PORE)*EXT)

      RETURN
      END
```